

IN 92

40123

p48

NASA Technical Memorandum 105216

Solar Radiation on Mars—Update 1991

(NASA-TM-105216) SOLAR RADIATION ON MARS:
UPDATE 1991 (NASA) 48 p CSCL 03B

N91-33046

Unclas
G3/92 0040123

✓ Joseph Appelbaum
National Aeronautics and Space Administration
Lewis Research Center
Cleveland, Ohio

and

✓ Geoffrey A. Landis
Sverdrup Technology, Inc.
Lewis Research Center Group
Brook Park, Ohio

September 1991

NASA

SOLAR RADIATION ON MARS - UPDATE 1991

Joseph Appelbaum*
National Aeronautics and Space Administration
Lewis Research Center
Cleveland, Ohio 44135

and

Geoffrey A. Landis
Sverdrup Technology, Inc.
Lewis Research Center Group
Brook Park, Ohio 44142

ABSTRACT

Detailed information on solar radiation characteristics on Mars are necessary for effective design of future planned solar energy systems operating on the surface of Mars. In this paper we present a procedure and solar radiation related data from which the daily variation of the global, direct beam and diffuse insolation on Mars are calculated. Given the optical depth of the Mars atmosphere, the global radiation is calculated from the normalized net flux function based on multiple wavelength and multiple scattering of the solar radiation. The direct beam was derived from the optical depth using Beer's law, and the diffuse component was obtained from the difference of the global and the direct beam radiation. The optical depths of the Mars atmosphere were derived from images taken of the Sun with a special diode on the cameras used on the two Viking Landers.

1. INTRODUCTION

Missions to the Martian surface will require electric power. Of the several possibilities, photovoltaic power systems can offer many advantages, including high power to weight, modularity, scalability, and a long history of successful application in space. To design a photovoltaic system, detailed information on solar radiation data on the Martian surface is necessary to allow more accurate estimates of photovoltaic power system size and mass in system analysis and trade-off studies of relevant technology options.

*National Research Council - NASA Research Associate; present address Tel Aviv University, Tel Aviv, 69978 Israel. Work funded under NASA grant NAGW-2022.

Solar irradiance on the Mars surface varies with season and with the amount of atmospheric dust. A major concern is the dust storms, which occur on both local and global scales, and their effect on solar array output. Global storms may persist for long periods of time, such that the requirement for energy storage quickly becomes much too large to be practical. However, as we have shown there is still an appreciable large diffuse component of sunlight available even at high optical depths of the Mars atmosphere, so that solar array operation is still possible. Mars may be considered "clear" most of the time for most places, but when the global storms occur, their effects are large.

The variation of the solar radiation on the Martian surface is governed by three factors: (1) the variation in Mars-Sun distance, (2) variation in solar zenith angle due to Martian season and time of day, and (3) opacity of the Martian atmosphere. Opacity measurements were derived from images taken of the Sun with a special diode on the cameras used on the two Viking Landers. Viking Lander 1 (VL1) is located at 22.3° N latitude and 47.9° W longitude (in Chryse) and Viking Lander 2 (VL2) is located at 47.7° N latitude and 225.7° W longitude (in Utopia). Mars maps can be found in [1]. The camera observations have produced 1044 measurements of optical depth spread over 1-1/3 Martian years.

The global solar radiation is composed of two components. The direct (or "beam") component is the light which comes directly from the Sun, attenuated by atmospheric dust. The diffuse component is the light reaching the surface from atmospheric scattering. Given the optical opacity, global radiation is calculated from the normalized net solar flux function based on multiple wavelength and multiple scattering of the solar radiation. The direct beam component was derived from the optical depth of the atmosphere using Beer's law, and the diffuse component was obtained from the difference of the global and direct radiation.

The Martian atmosphere consists mainly of suspended dust particles, the amount of which vary daily, seasonally, and annually, depending on local and global storm intensities and their duration. The intensity of the dust storms are defined in terms of the optical depth of the Martian atmosphere.

From a photovoltaic system design point of view, the intensity, frequency, and duration of these storms may be viewed as "partially cloudy" and "cloudy" days for which additional energy storage must be taken into account.

— This paper is an update to reference [2] and includes a refinement of the solar radiation model; Mars surface albedo; optical depths at different latitudes; and solar radiation data for the entire planet. The results are presented in a series of figures and tables. The solar radiation data and the procedure presented in this paper may be used for the calculation of any desired solar radiation quantity on Mars in an engineering design.

2. OPTICAL DEPTH AT VIKING LANDERS

The most direct and probably most reliable estimates of opacity are those derived from the Viking Lander imaging of the Sun. Figures 1 and 2 show the seasonal variation of the normal incidence of the optical depth at the Viking Lander locations VL1 and VL2, respectively. The season is indicated by the value of L_s , areocentric longitude of the Sun, measured in the orbital plane of the planet from its vernal equinox, $L_s = 0^\circ$. Figures 1 and 2 were derived from [3] and were discretized for each 5° (see measured and discretized). Opacities are minimum during the northern spring ($L_s = 0^\circ$ to 90°) and summer ($L_s = 90^\circ$ to 180°), and maximum during southern spring ($L_s = 180^\circ$ to 270°) and summer ($L_s = 270^\circ$ to 360°), the seasons during which most local and major dust storms occur. When dust storms are not present, the optical depth is typically about 0.5.

Two global dust storms occurred during the periods of each observation, as indicated by the high values of the optical depth (they are lower bound values). Numerous local dust storms were observed as well. Figures 3 and 4 show the variation of the optical depth of Figs. 1 and 2 in greater detail.

The cameras on the Viking Lander measured the optical depth in the morning and in the afternoon. The morning optical depths are higher, on the average, than the afternoon optical depths. These differences indicate a diurnal cycle of water condensation and evaporation. The afternoon

optical values are more representative of that solely due to the suspended dust particles. These values are shown in Figs. 1 and 2 and are assumed to remain constant throughout the day for the solar radiation calculation. Other methods [4,5] for the estimation of the optical depth of the Mars atmosphere deal with the solar reflected or thermally emitted radiation. The optical depth derived from the Viking Lander imaging of the Sun, which is used in the paper, is a direct method and is independent of the optical properties and temperatures of the ground and airborne dust.

3. OPTICAL DEPTH AT DIFFERENT LATITUDES

The optical depths at different latitudes other than the ones measured at the Viking Landers VL1 and VL2 are introduced in this article and are based on the assumption that the optical depth varies spatially and are expected to be greatest in the source region where dust is raised into the atmosphere. References [4,5] support this assumption. It is therefore assumed that the optical depths have a Gaussian distribution centered at the times of the global storms at VL1 and VL2. The relationship of the optical depth with latitudes may be expressed by a low order polynomial ratio. The optical depth function coefficients correspond to the measured opacities at VL1 and VL2. This function: $\tau(\phi, L_s)$, was developed for the case of two global dust storms per Martian year; a model that corresponds to the Viking Lander observation.

The location of the first global storm is well characterized, however there is some uncertainty about the location where the second 1977 storm started. We have therefore developed two models for global dust storm opacity, corresponding to latitude -10° and -30° locations for the second storm. The primary source areas for dust during the growth phases of global dust storms on Mars have historically been the Hellas and the Solis Planum regions. For the first model we thus assumed that the two global dust storms have originated both at latitude $\phi = -30^\circ$ and took place and at $L_{s1} = 215^\circ$ (first storm) and at $L_{s2} = 295^\circ$ (second storm). The model for the optical depth function, is assumed to have the form:

$$\tau(\phi, L_s) = \max \left\{ 0.5, \left[16,787 \frac{\left(1 + \frac{\phi}{150}\right)}{1,917 + (\phi + 38.27)^2} \left[0.779 e^{-(L_s-215)^2/730} + e^{-(L_s-295)^2/730} \right] \right] \right\} \quad (1)$$

i.e., the optical depth takes the greater value between 0.5 and the value in the square parenthesis. The numerical constants were determined by several conditions based on the Viking Lander measurements and least square fitting. Figures 5 and 6 describe the variation of the optical depth with latitude ϕ and areocentric longitude L_s based on Eq. (1).

Reference [6] states that the second 1977 storm was centered in the Valles Marineris area (10° S, 50° to 80° W). A second optical depth function was therefore developed with the first global storm at latitude $\phi_1 = -30^\circ$ and the second global storm at latitude $\phi_2 = -10^\circ$. The times of the storms were taken the same as before at $L_s = 215^\circ$ and $L_s = 295^\circ$. In this case, the optical depth function was assumed to have the following form:

$$\tau(\phi, L_s) = \max \left\{ 0.5, \left[19,500 \frac{\left(1 + \frac{\phi}{150}\right)}{4,000 + (\phi + 48.1)^2} e^{-(L_s-215)^2/730} + 12,700 \frac{\left(1 + \frac{\phi}{410}\right)}{2,465 + (\phi + 13.1)^2} e^{-(L_s-295)^2/730} \right] \right\} \quad (2)$$

i.e., the optical depth takes the greater value between 0.5 and the value in the square parenthesis. The numerical constants were determined similar to the preceding model. Figures 7 and 8 describe the variation of the optical depth with latitude ϕ and areocentric longitude L_s based on Eq. (2).

4. DUST STORMS

Observation from Earth, from orbit around Mars, and from the surface of the planet itself have shown that airborne dust is a highly variable and thermodynamically significant component of the Martian atmosphere. Martian dust plays a key role in determining the current climate of Mars, and is suspected of having a major influence on the evolution of the surface and the history of climatic

conditions on the planet. Airborne dust may be transported over short or long distance depending upon regional meteorological conditions. Dust is raised from the surface into the atmosphere, and when certain conditions are met, it may be translated into local or global dust storms. The spatial distribution of dust storms and of changes in surface albedo suggest that dust can be removed from the surface almost anywhere on the planet. There may be long periods when little dust moves at all at some locations, while there appear to be other regions where dust is raised more frequently. Many of the parameters controlling the location, severity, and frequency of dust-raising activity are not well understood. The classical view is that dust storm activity is correlated with a general intensification of winds around the time of maximum insolation, near southern summer solstice and perihelion. Dust storms are distinguished as minor or major storms, the former being localized clouds that remain locally and dissipate in a few days or so. Major dust storms are also called "global" or "great" storms and are classified as regional (do not encircle the planet) or planet-encircling (cover much of one or both hemispheres) storms. Local storms appear to play an important role in initiating the global storms. The thermodynamics of local storm generation and the mechanisms by which local storms become planet-encircling storms remain obscure. During the planet-encircling dust storms, dust is raised and spread over much of the planet for many Martian days (sols), and eventually falls to the surface. The direction of the dust transport of these storms is that dust is moved about within the southern hemisphere or from the south to the north over several weeks. The atmospheric dust decreases the amount of insolation reaching the surface, increases the infrared atmosphere heat flux, and absorb radiation emitted by the surface. A compilation record of all known clouds and dust activities on Mars reported in the literature over the past 115 years is reported in [7]. The characteristics of the global and local dust storms are discussed in the following subsections.

4.1 Global Dust Storms (Regional and Planet-Encircling Storms)

Global dust storms have been observed on Mars for many years, both from Earth-based telescope observations and from Mariner 9 and Viking spacecraft observations. These storms typically

develop during the southern summer season, presumably because wind speeds reach their peak at that time as the solar insolation is maximum at perihelion passage. The global dust storms appear to evolve from local storms in preferred regions. These regions - Claritas Fossae/Solis Planum, Hellespontus/Noachis, Sirtis Major Isidis (Fig. 9) - are characterized by their location in low and subtropical latitudes, by the presence of large east-west slopes, and by strong gradients in surficial albedo or thermal inertia. Global dust storms do not occur in northern spring and summer because of the greatly reduced insolation available at that time. Effects of major dust storms on the global opacity vary depending on the intensity and latitudinal extent of the storm. Initial buildup in opacity occurs over 2 weeks, decay begins immediately thereafter. The decay period of several months occurs between storms before a new storm is initiated. Although the major storms affected most of the planet, the latitudinal distribution is nonuniform. One or more dust storms of regional or larger size can occur in any given Mars year. There are many Mars years in which no planet-encircling dust storm has occurred; less frequently, there may be years in which not even regional storms occur. The duration of the global dust storms may vary from 35 to 70 days or more. The first global dust storm observed by Viking Landers (1977) spread from a latitude of 40° S to a latitude of 48° N in about 5 to 6 days. The first storm moved northward at a speed of 10 m/sec and the second storm moved northward at a speed of 30 m/sec. Figure 1 also shows the seasonal date L_s of those Martian great dust storms (identified by the year in which they occurred) whose regional onset was obtained from Earth and/or by spacecraft or by the Viking Landers. When more than one storm has occurred in a single (terrestrial year), they are designated a or b (as in 1977a) in the order of their appearance. As is noticed, the storms were observed in southern spring and summer [8].

4.2 Local Dust Storms

Three independent sources of information about local dust storms on Mars assess the spatial and temporal distribution of the clouds: (1) Viking Orbiter Infrared Thermal Mapper (IRTM); (2) Viking

Orbiter VIS (Visual Imaging Subsystem) data; and (3) the historical record of dust clouds occurrence produced from Earth-based telescopic observations [9].

Local dust storms, which may affect regions encompassing up to 10^6 km², have been observed on Mars during all seasons. However, they have been observed to occur most frequently in the approximate latitude belts 10° to 20° N and 20° to 40° S, with more clouds seen in the south than in the north and with more frequent sighting during southern spring and summer. Thus local storms are apparently most likely to occur during the same period as the global dust storms. The local storms are not uniformly distributed in latitude and season.

The local dust storms which Viking detected in the southern hemisphere can be divided into two groups: those occurring within 10° to 15° of latitude of the receding south polar cap and those in the 10° to 30° S latitude zone.

Common local dust storm localities in the southern hemisphere include: the region from Noctis Labyrinthus to Thaumasia Fossae, Argyre, Noachis-Hellespontus, Hellas, and the edge of the south polar cap. Common local dust storm sites in the northern hemisphere include: Chryse, Isidis-Syrtis Major, Cerberus, and Acidalia. Based on the number of observed clouds, an estimated 100 local storms occur annually. Most are associated with winds along the receding south polar cap and peak surface heating in the southern hemisphere near perihelion. Local dust storms form and dissipate in a few days or less. A statistical treatment of the local storms is given in the "Occurrence Probability of Local Dust Storms" section.

5. SURFACE ALBEDO

The albedo of a surface is a measure of the incident solar radiation reflected by the surface. The albedo behavior of Mars was measured by the Viking IRTM instruments in the range of 0.3 to 3.0 μ m [10]. Global dust storms on Mars play an important role in the deposition and removal of fine dust materials. The major variations in albedo were associated with the two global dust storms, of 1977. During the seasons that are free of global dust storms the observed albedo was reasonably

uniform. Between the two storms, the atmosphere cleared substantially with many southern hemisphere regions returning to their prestorm albedos. The northern hemisphere atmosphere retained dust longer during the decay phase of the storms than the southern hemisphere. Southern hemisphere dark regions were not measurably brighter following the global storm suggesting little net deposition of dust (rate less than 0.15 to $\sim 1.5 \mu\text{m}/\text{year}$). In contrast, the northern hemisphere dark regions of Syrtis Major and Acidalia Planitia were measurably brighter following the storms, indicating a deposition of dust. These surfaces subsequently darkened over the following months returning to prestorm albedo values. Dust is also deposited in bright, low-inertia regions (at a rate of a few to $\sim 45 \mu\text{m}/\text{year}$), where it remains. Remote sensing observations indicate that major dust deposits are currently located in three northern equatorial regions: Tharsis, Arabia and Elysium. They are covered by fine (~ 2 to $40 \mu\text{m}$) bright (albedo > 0.27) particles.

Considering solar collectors operation on the Martian surface in the context of dust deposition on the collectors and the change in the nearby surface albedo, we may take into account the following: the amount of solar radiation at perihelion and maximum wind velocities occur in the south causing storm initiation, whereas regional dust deposition occurs in the north suggesting net transport of dust from south to north. In the south, very small amounts of dust are deposited, whereas in the north there are regional dust deposits remaining on the surface for a length of time (few months), and there are regions where the dust accumulate and remain.

The variation of the surface albedo on Mars with latitude and longitude is given in Table I for each 10° and is based on [11]. The albedo is taken into account also in solar radiation calculation on tilted surfaces. The mean albedo on Mars is about 0.27 and the maximum value is about 0.4. Table I may be used for clear days. For periods with dust storms we introduce an albedo function given by:

$$al = \max\{al_T, \min(0.18\tau, 0.4)\} \quad (3)$$

where al_T is the albedo in Table I and 0.4 is the maximum albedo value. This function is based on the assumption that during dust storms the albedo increases above the value in Table I. It is also

assumed that dust storms that cause the atmospheric optical depth to increase above the value of 1.5 will increase the surface albedo above its mean value of 0.27; thus obtaining the value of 0.18 ($0.27/1.5 = 0.18$). A maximum value of 0.4 for the albedo is assumed regardless of the dust storm intensity.

6. MARS SEASONS

Mars has seasons comparable to those of Earth. However, the seasons are on the average about twice as long as on the Earth, corresponding to the greater length of the Martian year. Furthermore, they are distinctly unequal in duration as a result of the appreciable eccentricity of the Martian orbit. For that reason, the Martian year is not divided into months. Table II gives the duration of the Martian seasons in terrestrial and Martian days (a Martian day is defined as a sol, 1 sol = 24.65 hr). The Martian year is divided into degrees of areocentric longitudes, corresponding to the position of Mars in its orbit around the Sun. Areocentric longitudes $L_s = 0^\circ$ and 180° correspond to the spring and fall equinox for the northern hemisphere, respectively, and $L_s = 90^\circ$ and 270° correspond to northern and southern summer solstices, respectively. Figure 10 shows how many (terrestrial) days are in 1° of areocentric longitude. This relationship is based on Mars orbit and the law of conservation of the angular momentum and is given by:

$$d = \frac{687}{360} \frac{(1 - e^2)^{3/2}}{[1 + e \cos(L_s - 248^\circ)]} \quad (4)$$

7. SOLAR RADIATION AT THE TOP OF MARS ATMOSPHERE

The variation of the solar radiation at the top of the Mars atmosphere is governed by the location of Mars in its orbit and by the solar zenith angle. The solar radiation is direct beam radiation. The beam irradiance, in W/m^2 , is given by:

$$G_{ob} = \frac{S}{r^2} \quad (5)$$

where S is the solar constant at the mean Sun-Earth distance of 1 AU, i.e., $S = 1371 \text{ W/m}^2$; r is the instantaneous Sun-Mars distance in AU (heliocentric distance) given by [12]:

$$r = \frac{a(1 - e^2)}{1 + e \cos \theta} \quad (6)$$

where a is the Mars semi-major axis in AU, e is the Mars eccentricity ($e = 0.093377$) and θ is the true anomaly given by:

$$\theta = L_s - 248^\circ \quad (7)$$

where L_s is the areocentric longitude and 248° is the areocentric longitude of Mars perihelion. The Sun-Mars mean distance in astronomical units (AU) is 1.5236915; therefore, the mean beam irradiance at the top of the Martian atmosphere is: $1371/1.5236915^2 = 590 \text{ W/m}^2$. The instantaneous beam irradiance is given by Eqs. (5) to (7).

$$G_{ob} = 590 \frac{[1 + e \cos(L_s - 248)]^2}{(1 - e^2)^2} \quad (8)$$

8. SOLAR RADIATION ON THE SURFACE OF MARS

The variation of the solar radiation on the Martian surface is governed by three factors: (1) the Mars-Sun distance, (2) solar zenith angle, and (3) the opacity of the Martian atmosphere. The global solar irradiance G is the sum of the direct beam irradiance G_b , the diffuse irradiance G_d , and the albedo G_{al} :

$$G = G_b + G_d + G_{al} \quad (9)$$

The direct beam irradiance on the Martian surface normal to the solar rays is related by Beer's law to the optical depth, τ , of the intervening atmospheric haze:

$$G_b = G_{ob} \exp [-\tau m(z)] \quad (10)$$

where $m(z)$ is the air mass determined by the zenith angle z , and can be approximated, for zenith angles up to about 80° , by:

$$m(z) \approx \frac{1}{\cos z} \quad (11)$$

The zenith angle of the incident solar radiation is given by:

$$\cos z = \sin \phi \sin \delta + \cos \phi \cos \delta \cos \omega \quad (12)$$

where

ϕ latitude

δ declination angle

ω hour angle measured from the true noon westward

The solar declination angle is given by:

$$\sin \delta = \sin \delta_o \sin L_s \quad (13)$$

where $\delta_o = 24.936^\circ$ is the Mars obliquity of rotation axis. The ratio of Mars to Earth length of day is 24.65/24. It is convenient, for calculation purposes, to define a Mars hour, H , by dividing the Martian day (sol) into 24 hr. Using the same relationship between the Mars solar time T and the hour angle as for the Earth, we write:

$$\omega = 15T - 180 \quad (14)$$

This is shown in Fig. 11. The final solar radiation results can then be adjusted by the above ratio to correspond to actual (terrestrial) time. The sunset hour angle is given by [13]:

$$\omega_{ss} = \cos^{-1}(-\tan \phi \tan \delta) \quad (15)$$

if $|\phi| < \pi/2 - |\delta|$.

If $-\tan \delta \tan \phi > +1$
or $\phi < -\pi/2 + \delta$ or $\phi > \pi/2 + \delta$

the Sun will neither rise nor set for the day:
polar night

If $-\tan \delta \tan \phi = \pm 1$

the Sun will be on the horizon for an instant
only

(16)

If $-\tan \delta \tan \phi < -1$
or $\phi > \pi/2 - \delta$ or $\phi < \pi/2 - \delta$

the Sun will neither rise nor set for the day:
polar day

The number of Mars daylight hours is:

$$T_d = \frac{2}{15} \cos^{-1}(-\tan \phi \tan \delta) \quad (17)$$

and the actual (terrestrial) number of daylight hours is obtained by multiplying Eq. (17) by the ratio 24.65/24.

The solar irradiance on a horizontal Martian surface ($G_{al} = 0$) is given by:

$$G_h = G_{bh} + G_{dh} \quad (18)$$

where

G_h global irradiance on a horizontal surface

G_{bh} direct beam irradiance on a horizontal surface

G_{dh} diffuse irradiance on a horizontal surface

The diffuse irradiance of the Martian atmosphere may be a result of a mechanism different from that for the Earth atmosphere, nevertheless, to a first approximation, we will apply Eq. (18) as for Earth-terrestrial calculations.

The global irradiance G_h on a horizontal surface is given by:

$$G_h = G_{ob} \cos z \frac{f(z, \tau, al)}{1 - al} \quad (19)$$

where al is the albedo, and $f(z, \tau, al)$ is called the normalized net flux function. The net solar flux integrated over the solar spectrum on the Martian surface was calculated by Pollack [11] based on multiple wavelength and multiple scattering of the solar radiation. Derived data from this calculation

are shown in Tables III(a) and (b) for albedo = 0.1; and Tables IV(a) and (b) for albedo = 0.4. The parameters are the zenith angle z and the optical depth τ . For albedos between 0.1 and 0.4 a linear interpolation can be used. Figures 12 and 13 describe the variation of the normalized net flux function with optical depth and Sun zenith angle for 0.1 and 0.4 albedo, respectively, for some data in Tables III and IV. The normalized net flux function can be approximated by a polynomial expression given by:

$$f(z, \tau, al) = \left[\sum_{i=0}^5 \sum_{j=0}^5 \sum_{k=0}^1 p(i, j, k) \cdot \tau^i \cdot \left(\frac{z}{100} \right)^j \cdot (al)^k \right] (1 - al) \quad (20)$$

where $p(i, j, k)$ are the coefficients of the polynomial given in Table V. These coefficients were obtained from fitting Eq. (20) to the data in Tables III and IV based on the criteria of least square error. The mean error is about 0.7 percent for the full range. For zenith angles up to 40° the error is much smaller. The largest error is for zenith angle of 80° and 85° and for τ greater than 5. At these large angles and opacities, the error has a minor effect on the calculated daily insolation. The maximum error is about 7 percent.

Using Eqs. (10) and (11), the beam irradiance G_{bh} on a horizontal surface is given by:

$$G_{bh} = G_{ob} \cos z \exp\left(\frac{-\tau}{\cos z}\right) \quad (21)$$

and the diffuse irradiance is obtained by subtracting the beam from the global irradiances (Eqs. (19) and (21)). Figures 14 to 16 describe the variation of the global, beam and diffuse irradiances, respectively, on a horizontal Martian surface; and are given in pairs as functions of the optical depth τ and zenith angle z . The irradiances were calculated based on Tables III and IV data, the mean irradiance of 590 W/m^2 and mean albedo of 0.27. The variation of the global irradiance G_h , Eq. (19) is shown in Figs. 14(a) and (b). The beam irradiance G_{bh} is obtained using Eq. (21) and is shown in Figs. 15(a) and (b). The beam irradiance shows a sharp decrease with increasing of the optical depth, and a relative moderate decrease with increasing of the zenith angle. The diffuse irradiance G_{dh} is given in Figs. 16(a) and (b) and shows a sliding maximum with the variation of the zenith angle.

The solar radiation (global, beam and diffuse) variation (diurnally and daily) can be calculated based on the preceding equations and the $f(z, \tau, \alpha)$ function. For a given L_s and ϕ , one can calculate the variation of the zenith angle z as function of the Mars solar time T using Eqs. (12) and (14). Referring to Figs. 3 and 4 for the given L_s (or Eqs. (1) or (2)), the optical depth τ is determined. With the albedo value Eq. (3), Tables III and IV (or Eq. (20)), and Eqs. (18), (19) and (21), one can calculate the solar radiation variation for the given day. The diurnal variation of the solar irradiances on a horizontal surface for $L_s = 141^\circ$ and $L_s = 295^\circ$ for Viking Lander location VL1 are shown in Figs. 17(a) and (b), respectively. Areocentric longitude $L_s = 141^\circ$ corresponds to the lowest opacity of 0.35, and $L_s = 291^\circ$ to the highest opacity of 3.6 (Fig. 3). The figures show clearly that at high opacity, the diffuse component dominates the solar radiation. The daily global insolation H_h , beam insolation H_b and diffuse insolation H_d can be calculated by integrating the irradiances over the period from sunrise to sunset. Figures 18(a) and (b) shows the daily global insolation H_h on a horizontal surface, in kWhr/m²-day at VL1 and VL2 over a Martian year. The albedo at VL1 is 0.22 and at VL2 is 0.24. Also shown is the percentage of the diffuse insolation H_{dh}/H_h on a horizontal surface. During the spring and summer where the optical depth is relatively low, the diffuse insolation comprises about 50 percent of the global insolation, whereas for autumn and winter, the optical depth is high and therefore the diffuse insolation is about 90 percent.

A different view on the amount of solar radiation on Mars is the cumulative irradiance for the entire year. This is presented in Fig. 19. The ordinate is the instantaneous irradiance and the abscissa is the percent of yearly sunshine hours. The figure shows, for example, that during about 55 percent of the yearly sunshine hours the irradiance on a horizontal surface at VL1 is above 200 W/m².

The variation of the daily average irradiance in W/m² and the daily insolation in Whr/m²-day on a horizontal surface for the entire planet (for latitudes other than for the Viking Landers) will now be given based on the models of the optical depth functions, $\tau(\phi, L_s)$, Eqs. (1) and (2). The average irradiance is obtained by dividing the insolation value by the number of daylight hours for the given

day, Eq. (17). The variation of the global irradiance, G_h , with latitude ϕ and areocentric longitude L_s on a horizontal surface using Eq. (1) is shown in Fig. 20, and the daily global insolation, H_h , is shown in Fig. 21. The variation of G_h and H_h on a horizontal surface using Eq. (2) is shown in Figs. 22 and 23, respectively.

The two global dust storms that were observed in 1977 may be considered as one of the worst years of dust activities on Mars. However, there are many Mars years in which no global storm occurred. In Fig. 24 we compare the daily global insolation at VL1 and VL2 for the observed opacities in 1977 (see Figs. 3 and 4) and for an assumed Martian year with no global dust storms and with a constant optical depth of $\tau = 0.5$.

9. OCCURRENCE PROBABILITY OF LOCAL DUST STORMS

Local dust storms may be related to clouds and hazes of the Mars atmosphere. The occurrence of the local dust storms is of statistical nature and, therefore, has to be treated accordingly. The estimation of the occurrence probability of these storms at a given location on Mars is based on Table 3 of [14]. The clouds and hazes in percentages are given in [14] for 6 latitude and 10 seasonal bins. The hazes are divided into three categories according to the visibility of surface features through the obscuration. "Thin" haze (visible optical depth $\tau < 1$); "moderate" haze ($\tau \approx 1$); and "thick" haze ($\tau > 1$). Each hemisphere is divided into three latitude bins: equatorial, 0° to 30° latitude, mid-latitude, 30° to 60° ; and polar, 60° to 90° . The season bins, include 0° to 45° , 45° to 80° , 80° to 125° , 125° to 160° , 160° to 200° , 200° to 245° , 245° to 270° , 270° to 290° , 290° to 325° , and 325° to 360° of areocentric longitude L_s . The occurrence probability P was defined as the number of clouds or hazes divided by the number of observations for a given period of time. Based on this information we developed a statistical model for the occurrence of the local dust storms. All three types of hazes were combined into a single probability number. The clouds were not considered since they are usually smaller in spatial extent. The occurrence probability in [14] reports on clouds and hazes seen by Viking observers in a given bin area. Our purpose is to translate these events into an

occurrence probability as seen by an observer on Mars surface. Since the area of a bin is large, a cloud occurrence in this bin may not be detected by an observer on the surface. In order to estimate the occurrence probability of a local dust storm affecting an area on Mars surface, the probability P has to be normalized with respect to areas, i.e.,

$$P_r = P \frac{A}{A_{\bullet}} \quad (22)$$

where A is the area covered by a local dust storm, and A_{\bullet} is the bin area given by:

$$A_{\bullet} = 2\pi R^2 (\sin\phi_1 - \sin\phi_2) \quad (23)$$

where R is the Mars radius, and ϕ_1 and ϕ_2 are the latitudes defining the bin. Table VI gives the occurrence probability P_r (in percentage) for a local dust storm covering an area A of 10^5 km^2 for the given latitudinal and seasonal bins.

9.1 Occurrence Probability of a Number of Local Dust Storms

It is possible to estimate the occurrence probability $P(N)$ of local dust storms for a given length of time t at a given location. This is given by:

$$E[P(N)] = P_r \frac{t}{t_s} \quad (24)$$

where $E[P(N)]$ is the expected value of the occurrence for local dust storms and t_s is their duration.

To calculate the occurrence of N storms, $P(N)$, we assume a Poisson distribution where an occurrence of a storm is independent on the occurrence of subsequent storms, i.e.,

$$P(N) = k^N \quad (25)$$

For an observation time t equals to the duration time t_s of the local storm it is possible to show that

$$E[P(N)] = E(k^N) = P_r = \left(\frac{1}{1-k} \right)^2 k \quad (26)$$

or

$$k = \frac{2P_r + 1 - \sqrt{4P_r + 1}}{2P_r} \quad (27)$$

where k is the occurrence probability for one local storm in the period $t = t_s$. Small values of P_r (Eq. (27)) yields $k \approx P_r$, i.e., the occurrence probability of one local dust storm is given by P_r in Table VI. The greatest probability as indicated in (Table 3, [14]) is for the latitudinal bin -90° to -60° and seasonal bin 245° to 270° . According to Table VI, $P_r = 0.06852$ and from Eq. (24) $k = 0.0607$, i.e., $k \approx P_r$. The occurrence probability of a local dust storm is (Eq. (25)) $P(1) = k$, i.e., 6.07 percent. The occurrence probability of two storms is $P(2) = k^2 = 0.0037$.

Local dust storms may be taken into account in solar radiation calculation. The occurrence probability P_r represents the local dust storms in the solar radiation calculation. It is used for the optical depth models for latitudes other than for the measured values at the Viking Landers VL1 and VL2. This is because the measured optical depths already contain the effect of the local storms, if they really occurred. To determine whether a local dust storm occurred for a given latitude ϕ and day L_s , a number is randomly selected in the range between 0.0 and 1.0. If the value P_r in Table VI is greater than the randomly selected number we assume that there is a local dust storm. The models for the optical depths assumes $\tau = 0.5$ for clear skies. The optical depth for a local storm is taken as $\tau = 1$. The effect of the local dust storms on the daily global insolation H_h on a horizontal surface is calculated according to:

$$\overline{H_h} = H_{h|_{\tau=0.5}} (1 - P_r) + H_{h|_{\tau=1.0}} \cdot P_r \quad (28)$$

where P_r is given in Table VI.

An example of this calculation is shown in Fig. 25. The latitude $\phi = -70^\circ$ (i.e., very far south) was selected for the calculation because this region is most affected by local storms. In order to exaggerate the effect, the dust storm probability was arbitrarily doubled over that in Table VI. The assumed optical depth τ was 0.5 and for a year without global dust storms. For comparison purpose Fig. 25 also shows the curve for $\tau = 1.0$, showing the insolation during a local dust storm. The effect of the local dust storms is noticed by comparing H_h for $\tau = 0.5$ with the $\overline{H_h}$. The largest effect, in

this example, is 1.3 percent for $L_s = 265$. On the average, local dust storms have a minor effect on the daily global insolation.

9.2 Number of Days with a Local Dust Storm in a Year at a Given Location

Local dust storms may be taken into account in sizing the capacity of the energy storage. Days with local dust storms may be considered as days with low irradiance or "dark days." The number of days, in units of L_s , in a Martian year with local dust storms may be determined for each latitudinal bin $\Delta\phi$ by:

$$d_{ts} = \sum_{\Delta L_s} P_r(\Delta\phi, \Delta L_s) \times \Delta L_s \quad (29)$$

where ΔL_s is the seasonal bin. This is presented in Table VII.

If the duration of a local dust storm is 5° of L_s , the number of local dust storms for each latitudinal bin per year is obtained by dividing the values in Table VII by 5° .

CONCLUSIONS

The solar radiation model for Mars has been refined to include an extension of the net solar flux function $f(z, \tau, al)$, surface albedo, optical depth function for different latitudes and a statistical treatment of local dust storms. The paper presents a procedure and solar radiation related data from which the diurnally and daily variation of solar radiation on Mars were calculated.

The two global dust storms that were observed in 1977 make it one of the worst years of dust activities. Even so, the opacities are relatively low during the northern spring and summer for more than a half Martian year (or more than a terrestrial year) for which the insolation is relatively high varying from about 2 to 4 kWhr/m²-day. These seasons are the likely ones during which manned missions may be carried out. It should also be noted that there are many Mars years in which no planet-encircling dust storm has occurred; less frequently, there may be years in which not even regional storms occur. One of the most important results of this study is that there is a large diffuse component of the solar insolation, even at high opacity, so that solar energy system operation is still possible.

The insolation model for Mars presented in this paper enables more accurate engineering studies and estimates of solar cell array size and performance than has heretofore been possible.

ACKNOWLEDGMENT

We are very grateful to James B. Pollack from the Space Science Division, NASA Ames Research Center for supplying us with the data from which the $f(z,\tau,al)$ tables were derived.

We thank the Department of the Interior - U.S. Geological Survey for supplying us with Mars Map, Fig. 11.

We are very grateful to I. Sherman - student of Tel Aviv University, Israel for the computer programs and graphs.

Thanks are extended to Dr. Dennis J. Flood - NASA Lewis Research Center and coauthor of reference [2] for initiating the project and for his support.

This work was funded by NASA grant NAGW-2022.

NOMENCLATURE

A	area covered by a local storm
al	Mars surface albedo
d	number of terrestrial days
d_{ts}	number of days (in units of L_s) of local dust storms
G_b	beam irradiance on Mars surface
G_h, G_{bh}, G_{dh}	global, beam and diffuse irradiance on Mars horizontal surface
G_{ob}	beam irradiance at the top of Mars atmosphere
H_h, H_{bh}, H_{dh}	global, beam and diffuse daily insolation on Mars horizontal surface
Subscripts:	
b	direct (beam) values
d	diffuse values
h	horizontal values
o	values on top of Mars atmosphere
Other values:	
e	eccentricity = 0.093377
k	occurrence probability for one local storm

L_s	areocentric longitude (position of Mars in orbit around the Sun)
$m(z)$	air mass
r	Sun-Mars distance
R	Mars radius
S	solar constant = 1371 W/m^2 at the mean Sun-Earth distance of 1 astronomical unit (AU)
T	Mars solar time
t	time
t_s	duration of a local storm
P_r	occurrence probability of a local storm
$P(N)$	occurrence probability of local storms
T_d	Mars daylight hours
z	zenith angle
δ	declination angle
δ_o	obliquity
θ	true anomaly
τ	optical depth
ϕ	latitude
ω	hour angle
ω_{ss}	sunset hour angle

REFERENCES

- [1] J. Blunck, Mars and its Satellites, Exposition Press, 1982.
- [2] J. Appelbaum, D.J. Flood, "Solar Radiation on Mars' Solar Energy," Vol. 45, No. 6, pp. 353-363, 1990.
- [3] D.S. Colburn, J.B. Pollack, R.M. Haberle, "Diurnal Variation in Optical Depth at Mars," ICARUS, Vol. 79, pp. 159-189, 1989.
- [4] T. E. Torpe, "A History of Mars Atmospheric Opacity in the Southern Hemisphere During the Viking Extended Mission," J. Geophysical Research, Vol. 84, No. A11, pp. 6663-6683, 1979.
- [5] T.Z. Martin, "Thermal Infrared Opacity of the Mars Atmosphere," ICARUS, Vol. 66, pp. 2-21, 1986.
- [6] J.A. Ryan, R.M. Henry, "Mars Atmospheric Phenomena During Major Dust Storms, as Measured at Surface," J. Geophysical Research, Vol. 84, No. B6, pp. 2821-2829, 1979.
- [7] L.J. Martin, A History of Mars Dust Activity: A Composite List, Final Report JPL D-7257, Mar. 1990.
- [8] R.W. Zurek, "Martian Great Dust Storms: An Update," ICARUS, Vol. 50, pp. 258-310, 1982.
- [9] A.R. Peterfreund, Contemporary Aeolian Processes on Mars: Local Dust Storms, Ph.D. Thesis, Arizona State University, May 1985.
- [10] P.R. Christensen, "Global Albedo Variation on Mars: Implication for Active Aeolian Transport, Deposition and Erosion," J. Geophysical Research, Vol. 93, No. B7, pp. 7611-7624, 1988.
- [11] J.B. Pollack, et al., "Simulation of the General Circulation of Martian Atmosphere I: Polar Processes," J. Geophysical Research, Vol. 95, No. B2, pp. 1447-1473, 1990.
- [12] E.V.P. Smith, K.C. Jacob, Introductory Astronomy and Astrophysics, W.B. Saunders Co., 1973.
- [13] J.A. Duffie, W.A. Beckman, Solar Engineering of Thermal Processes, Wiley, 1980.
- [14] R. Kahn, "The Spacial and Seasonal Distribution of Martian Clouds and Some Meteorological Implications," J. Geophysical Research, Vol. 89, No. A8, pp. 6671-6688, 1984.

TABLE I. - MARS SURFACE ALBEDO

Longitude	Latitude, ϕ , deg																		
	-90	-80	-70	-60	-50	-40	-30	-20	-10	0	10	20	30	40	50	60	70	80	90
E 180	0.375	0.245	0.230	0.175	0.200	0.200	0.200	0.225	0.255	0.275	0.275	0.275	0.265	0.255	0.235	0.210	0.230	0.340	0.400
170	.375	.245	.230	.175	.200	.200	.195	.210	.250	.270	.270	.270	.270	.260	.235	.200	.230	.340	.400
160	.375	.245	.230	.175	.205	.200	.190	.195	.240	.265	.270	.270	.270	.265	.235	.200	.230	.340	.400
150	.375	.245	.230	.180	.210	.210	.185	.180	.225	.255	.265	.265	.275	.270	.235	.200	.230	.340	.400
140	.375	.245	.230	.185	.220	.225	.185	.175	.200	.250	.260	.260	.275	.270	.235	.210	.235	.365	.410
130	.375	.245	.230	.185	.225	.230	.190	.175	.190	.235	.250	.255	.265	.265	.230	.200	.250	.425	.425
120	.375	.245	.230	.190	.240	.235	.195	.175	.185	.225	.240	.240	.250	.260	.225	.190	.250	.430	.425
110	.375	.245	.230	.190	.240	.235	.195	.175	.175	.210	.230	.235	.250	.250	.220	.185	.250	.430	.425
100	.375	.245	.230	.195	.230	.225	.190	.175	.175	.200	.225	.230	.250	.248	.190	.175	.250	.430	.425
90	.375	.245	.230	.195	.230	.225	.200	.175	.170	.175	.175	.210	.240	.245	.200	.175	.250	.430	.425
80	.375	.245	.230	.200	.245	.250	.225	.175	.160	.150	.150	.185	.230	.248	.210	.185	.250	.425	.425
70	.375	.245	.230	.200	.250	.265	.225	.175	.160	.150	.150	.210	.245	.250	.225	.190	.250	.425	.425
60	.375	.245	.230	.200	.250	.265	.225	.180	.170	.175	.180	.250	.255	.255	.227	.200	.235	.400	.420
50	.400	.245	.230	.195	.240	.250	.225	.180	.185	.220	.240	.270	.260	.250	.230	.210	.230	.365	.410
40	.450	.250	.230	.190	.225	.225	.190	.180	.200	.250	.265	.270	.265	.250	.230	.210	.230	.340	.400
30	.450	.300	.230	.185	.215	.220	.190	.190	.210	.250	.275	.275	.265	.250	.230	.210	.230	.340	.400
20	.450	.300	.230	.180	.205	.215	.195	.200	.210	.245	.270	.275	.265	.250	.230	.210	.230	.340	.400
10	.450	.300	.230	.175	.200	.210	.195	.205	.200	.220	.250	.265	.252	.250	.225	.210	.230	.340	.400
0	.450	.300	.230	.175	.200	.205	.190	.190	.185	.200	.230	.245	.235	.220	.200	.200	.230	.340	.400
10	.450	.300	.230	.175	.200	.205	.185	.182	.180	.200	.220	.230	.220	.185	.160	.175	.230	.340	.400
20	.450	.300	.230	.180	.200	.200	.180	.175	.175	.200	.220	.210	.185	.150	.135	.150	.230	.340	.400
30	.450	.300	.230	.180	.205	.200	.175	.170	.175	.200	.225	.210	.175	.135	.125	.150	.230	.340	.400
40	.450	.300	.230	.180	.205	.200	.170	.170	.175	.210	.230	.225	.185	.150	.135	.150	.230	.340	.400
50	.400	.250	.230	.180	.205	.200	.175	.170	.175	.215	.240	.225	.210	.200	.175	.170	.230	.340	.400
60	.375	.245	.230	.175	.200	.195	.185	.175	.190	.225	.245	.235	.230	.235	.225	.190	.230	.340	.400
70	.375	.245	.230	.175	.190	.195	.185	.180	.205	.270	.285	.277	.277	.275	.255	.225	.235	.340	.400
80	.375	.245	.230	.175	.185	.190	.185	.190	.225	.285	.300	.285	.280	.275	.262	.230	.235	.340	.400
90	.375	.245	.230	.175	.180	.190	.185	.190	.250	.300	.300	.290	.287	.275	.270	.235	.235	.340	.400
100	.375	.245	.230	.175	.175	.190	.185	.200	.260	.295	.295	.288	.285	.275	.275	.240	.235	.340	.400
110	.375	.245	.230	.175	.175	.190	.185	.215	.270	.290	.290	.285	.280	.275	.262	.225	.230	.340	.400
120	.375	.245	.230	.175	.175	.190	.180	.230	.275	.280	.285	.280	.280	.277	.255	.220	.230	.340	.400
130	.375	.245	.230	.175	.185	.200	.190	.240	.275	.280	.280	.280	.277	.275	.255	.220	.230	.340	.400
140	.375	.245	.230	.175	.195	.200	.200	.235	.275	.275	.280	.280	.272	.270	.250	.220	.230	.340	.400
150	.375	.245	.230	.175	.200	.200	.200	.225	.265	.275	.275	.275	.265	.265	.250	.215	.230	.340	.400
160	.375	.245	.230	.175	.200	.200	.200	.225	.260	.275	.275	.275	.265	.260	.240	.210	.230	.340	.400
170	.375	.245	.230	.175	.200	.200	.200	.225	.260	.275	.275	.275	.265	.260	.240	.210	.230	.340	.400
W 180	.375	.245	.230	.175	.200	.200	.200	.225	.255	.275	.275	.275	.265	.255	.235	.210	.230	.340	.400

TABLE II. - MARS SEASONS

Areocentric longitude of the Sun, L_s , deg	Season		Duration of the season Mars	
	Northern hemisphere	Southern hemisphere	Martian days	Terrestrial days
0 to 90	Spring	Autumn	194	199
90 to 180	Summer	Winter	177	182
180 to 270	Autumn	Spring	142	146
270 to 360	Winter	Summer	<u>156</u>	<u>160</u>
			669	687

TABLE III(a). - NORMALIZED NET FLUX FUNCTION $f(z, \tau, al)$
AT THE MARTIAN SURFACE

Albedo 0.1									
Optical depth, τ	Zenith angle z , deg								
	0	5	10	15	20	25	30	35	40
0.10	0.883	0.883	0.883	0.882	0.881	0.880	0.879	0.877	0.875
.15	.875	.875	.874	.873	.872	.870	.868	.866	.862
.20	.866	.866	.865	.864	.862	.860	.857	.854	.850
.25	.857	.857	.856	.854	.852	.849	.846	.842	.838
.30	.848	.848	.847	.845	.842	.839	.835	.831	.826
.35	.839	.839	.838	.836	.833	.829	.824	.819	.813
.40	.830	.830	.829	.826	.823	.819	.814	.808	.801
.45	.822	.821	.820	.817	.814	.809	.804	.797	.790
.50	.813	.813	.811	.808	.804	.799	.793	.786	.778
.55	.805	.804	.802	.799	.795	.789	.783	.775	.767
.60	.796	.795	.793	.790	.785	.779	.772	.764	.755
.65	.787	.786	.784	.780	.775	.769	.762	.754	.743
.70	.778	.777	.775	.771	.766	.759	.752	.743	.732
.75	.770	.768	.766	.762	.757	.750	.742	.733	.721
.80	.761	.760	.757	.753	.748	.741	.732	.722	.711
.85	.752	.751	.748	.744	.739	.731	.722	.712	.701
.90	.744	.743	.740	.736	.730	.722	.713	.703	.690
.95	.736	.735	.732	.727	.721	.713	.703	.693	.680
1.00	.728	.727	.724	.719	.712	.704	.694	.683	.669
1.05	.720	.719	.716	.711	.704	.695	.685	.673	.659
1.10	.712	.711	.708	.703	.696	.687	.676	.664	.649
1.15	.704	.703	.700	.695	.688	.678	.667	.655	.640
1.20	.695	.694	.691	.686	.679	.669	.658	.645	.630
1.25	.687	.686	.683	.678	.670	.660	.649	.636	.621
1.30	.679	.678	.675	.670	.662	.652	.640	.627	.611
1.35	.672	.671	.668	.662	.654	.644	.632	.619	.602
1.40	.664	.663	.660	.654	.646	.636	.624	.611	.594
1.45	.657	.655	.652	.646	.638	.627	.615	.602	.585
1.50	.649	.648	.644	.638	.630	.619	.607	.593	.576
1.55	.642	.640	.637	.631	.622	.612	.599	.585	.568
1.60	.634	.633	.629	.623	.615	.604	.591	.577	.559
1.65	.627	.625	.621	.615	.607	.596	.583	.568	.551
1.70	.619	.618	.614	.608	.599	.588	.575	.560	.542
1.75	.612	.611	.607	.601	.592	.581	.568	.553	.534
1.80	.605	.604	.600	.594	.585	.574	.561	.546	.527
1.85	.598	.597	.593	.587	.578	.567	.553	.538	.520
1.90	.591	.590	.586	.580	.571	.559	.546	.531	.513
1.95	.584	.583	.579	.573	.564	.552	.539	.524	.506
2.00	.578	.576	.572	.566	.557	.546	.532	.517	.498
2.10	.564	.563	.558	.552	.543	.532	.518	.502	.483
2.20	.551	.549	.545	.539	.530	.518	.504	.489	.469
2.30	.538	.537	.533	.526	.517	.505	.492	.476	.457
2.40	.526	.524	.520	.514	.505	.493	.479	.464	.444
2.50	.514	.512	.508	.502	.493	.481	.467	.451	.432
2.60	.501	.499	.496	.489	.480	.468	.454	.438	.420
2.70	.489	.487	.483	.477	.468	.456	.441	.426	.407
2.80	.478	.477	.473	.466	.456	.445	.431	.415	.395
2.90	.467	.466	.462	.455	.446	.435	.421	.405	.385
3.00	.457	.456	.452	.445	.436	.425	.411	.395	.376
3.20	.436	.435	.431	.425	.416	.405	.391	.375	.357
3.40	.415	.414	.410	.404	.395	.384	.371	.356	.338
3.60	.395	.393	.389	.384	.376	.365	.352	.337	.319
3.80	.378	.376	.372	.367	.359	.349	.336	.321	.304
4.00	.363	.361	.357	.352	.344	.334	.321	.307	.290
4.50	.325	.323	.320	.315	.307	.297	.286	.272	.257
5.00	.289	.288	.285	.280	.273	.264	.253	.241	.227
5.50	.257	.256	.253	.249	.242	.234	.225	.213	.201
6.00	.229	.227	.224	.220	.215	.209	.200	.189	.178

TABLE III(b). - NORMALIZED NET FLUX FUNCTION $f(z, \tau, \alpha)$
AT THE MARTIAN SURFACE

Albedo 0.1									
Optical depth, τ	Zenith angle z , deg								
	45	50	55	60	65	70	75	80	85
0.10	0.872	0.868	0.862	0.855	0.844	0.830	0.804	0.757	0.640
.15	.858	.852	.844	.834	.819	.798	.762	.700	.566
.20	.844	.836	.826	.813	.794	.768	.724	.651	.508
.25	.831	.821	.808	.793	.770	.739	.688	.608	.466
.30	.818	.806	.791	.773	.747	.712	.656	.571	.433
.35	.804	.791	.774	.754	.726	.687	.627	.539	.407
.40	.790	.776	.758	.736	.706	.663	.599	.510	.385
.45	.778	.762	.742	.718	.686	.641	.575	.485	.367
.50	.765	.748	.727	.701	.667	.619	.551	.462	.351
.55	.753	.734	.712	.684	.648	.598	.528	.440	.337
.60	.741	.721	.697	.668	.631	.579	.508	.422	.325
.65	.728	.708	.683	.653	.615	.562	.491	.407	.315
.70	.716	.695	.669	.638	.600	.546	.474	.393	.306
.75	.705	.682	.655	.623	.585	.530	.457	.379	.297
.80	.693	.670	.642	.609	.570	.514	.442	.366	.288
.85	.682	.658	.630	.596	.556	.500	.429	.356	.281
.90	.671	.646	.617	.583	.543	.486	.416	.345	.274
.95	.660	.634	.605	.570	.528	.472	.403	.335	.267
1.00	.649	.623	.593	.557	.514	.459	.392	.324	.261
1.05	.638	.613	.582	.546	.503	.448	.382	.316	.255
1.10	.628	.602	.571	.535	.492	.438	.374	.309	.250
1.15	.618	.592	.561	.524	.480	.427	.364	.302	.245
1.20	.608	.581	.550	.513	.469	.416	.355	.295	.240
1.25	.598	.570	.539	.502	.457	.405	.346	.287	.235
1.30	.588	.560	.528	.491	.446	.395	.337	.280	.230
1.35	.579	.551	.519	.482	.437	.387	.331	.275	.226
1.40	.571	.542	.510	.473	.429	.379	.324	.270	.222
1.45	.562	.533	.501	.464	.420	.372	.318	.265	.219
1.50	.553	.524	.492	.455	.412	.364	.312	.260	.215
1.55	.544	.515	.483	.446	.403	.356	.305	.255	.211
1.60	.535	.506	.474	.437	.394	.348	.298	.249	.207
1.65	.527	.497	.465	.428	.385	.340	.292	.244	.203
1.70	.518	.489	.457	.420	.378	.333	.286	.240	.200
1.75	.511	.482	.450	.413	.371	.327	.281	.236	.197
1.80	.504	.475	.443	.406	.364	.321	.276	.232	.194
1.85	.496	.468	.436	.399	.358	.316	.272	.228	.191
1.90	.489	.460	.428	.392	.352	.310	.267	.225	.188
1.95	.482	.453	.421	.385	.345	.304	.262	.221	.185
2.00	.474	.445	.413	.377	.338	.298	.257	.217	.182
2.10	.459	.431	.399	.364	.325	.287	.248	.210	.176
2.20	.446	.417	.386	.352	.314	.276	.239	.203	.170
2.30	.433	.405	.374	.341	.304	.268	.232	.197	.166
2.40	.421	.393	.362	.330	.295	.260	.226	.192	.161
2.50	.409	.381	.351	.319	.285	.252	.219	.187	.157
2.60	.396	.369	.339	.308	.276	.243	.212	.181	.153
2.70	.384	.357	.328	.298	.266	.235	.205	.176	.148
2.80	.373	.347	.318	.289	.258	.228	.199	.171	.144
2.90	.363	.338	.310	.281	.251	.222	.193	.166	.140
3.00	.354	.329	.301	.273	.244	.216	.188	.162	.137
3.20	.336	.311	.285	.258	.231	.205	.179	.154	.131
3.40	.317	.294	.268	.243	.218	.193	.169	.146	.124
3.60	.299	.277	.253	.230	.206	.182	.160	.138	.117
3.80	.284	.263	.241	.218	.196	.174	.153	.132	.112
4.00	.271	.251	.229	.208	.187	.166	.146	.127	.107
4.50	.240	.222	.203	.184	.166	.148	.131	.114	.096
5.00	.212	.196	.179	.162	.146	.131	.116	.101	.086
5.50	.187	.173	.158	.143	.130	.116	.103	.090	.077
6.00	.166	.154	.141	.128	.116	.104	.093	.081	.069

TABLE IV(a). - NORMALIZED NET FLUX FUNCTION $f(z, \tau, al)$
AT THE MARTIAN SURFACE

Albedo 0.4									
Optical depth, τ	Zenith angle z , deg								
	0	5	10	15	20	25	30	35	40
0.10	0.596	0.595	0.594	0.593	0.592	0.591	0.590	0.589	0.588
.15	.592	.590	.590	.589	.588	.586	.585	.583	.582
.20	.587	.586	.585	.584	.583	.581	.579	.577	.575
.25	.583	.582	.581	.579	.578	.576	.574	.571	.569
.30	.578	.577	.576	.575	.573	.571	.568	.565	.562
.35	.574	.573	.572	.570	.568	.565	.563	.559	.556
.40	.569	.568	.567	.565	.563	.560	.557	.553	.549
.45	.565	.564	.563	.560	.558	.555	.552	.547	.542
.50	.560	.559	.558	.556	.553	.550	.546	.541	.535
.55	.555	.555	.553	.551	.548	.544	.540	.535	.529
.60	.550	.549	.548	.546	.543	.539	.534	.529	.522
.65	.545	.544	.543	.541	.538	.533	.528	.522	.516
.70	.540	.540	.538	.536	.532	.527	.522	.516	.509
.75	.535	.535	.533	.531	.527	.522	.516	.510	.503
.80	.531	.530	.528	.526	.522	.517	.511	.504	.496
.85	.526	.525	.523	.520	.517	.511	.505	.498	.490
.90	.521	.520	.518	.515	.511	.505	.499	.492	.483
.95	.516	.515	.514	.510	.506	.500	.494	.486	.476
1.00	.511	.511	.509	.506	.501	.495	.488	.480	.470
1.05	.506	.506	.504	.500	.496	.489	.482	.474	.464
1.10	.501	.501	.499	.495	.490	.483	.476	.468	.458
1.15	.497	.496	.494	.490	.485	.478	.471	.462	.452
1.20	.492	.491	.489	.485	.480	.473	.465	.456	.446
1.25	.487	.486	.484	.480	.475	.467	.460	.450	.439
1.30	.482	.481	.479	.475	.469	.462	.454	.445	.433
1.35	.477	.476	.474	.470	.464	.457	.449	.439	.428
1.40	.472	.471	.469	.465	.459	.452	.444	.434	.422
1.45	.467	.467	.465	.460	.455	.447	.438	.429	.417
1.50	.463	.462	.460	.456	.450	.442	.433	.423	.411
1.55	.458	.457	.455	.451	.445	.437	.428	.418	.406
1.60	.453	.452	.450	.446	.440	.432	.423	.413	.400
1.65	.449	.448	.445	.441	.435	.427	.418	.407	.395
1.70	.444	.443	.440	.436	.430	.422	.413	.402	.389
1.75	.440	.438	.435	.431	.425	.418	.408	.397	.384
1.80	.435	.434	.431	.427	.421	.413	.403	.392	.379
1.85	.431	.429	.427	.422	.416	.408	.398	.388	.375
1.90	.426	.425	.422	.417	.411	.403	.394	.383	.370
1.95	.422	.420	.418	.413	.406	.398	.389	.378	.365
2.00	.417	.416	.413	.408	.402	.394	.384	.373	.360
2.10	.408	.407	.404	.399	.393	.385	.375	.364	.350
2.20	.399	.398	.395	.391	.384	.376	.366	.355	.341
2.30	.391	.390	.387	.382	.376	.368	.358	.346	.332
2.40	.383	.382	.379	.374	.368	.359	.349	.338	.324
2.50	.375	.374	.371	.367	.360	.351	.341	.330	.316
2.60	.367	.365	.363	.358	.352	.343	.333	.321	.308
2.70	.358	.357	.354	.350	.343	.334	.324	.313	.299
2.80	.350	.349	.346	.342	.335	.326	.316	.305	.291
2.90	.343	.342	.339	.334	.328	.320	.310	.298	.284
3.00	.336	.335	.332	.327	.321	.313	.303	.291	.277
3.20	.322	.321	.318	.314	.307	.299	.289	.277	.264
3.40	.308	.307	.304	.300	.293	.285	.275	.264	.251
3.60	.294	.293	.290	.286	.280	.271	.262	.251	.238
3.80	.282	.281	.278	.274	.268	.260	.251	.239	.227
4.00	.271	.270	.267	.263	.257	.249	.240	.229	.217
4.50	.244	.243	.241	.237	.231	.224	.215	.205	.194
5.00	.219	.218	.216	.212	.207	.200	.192	.183	.173
5.50	.196	.196	.194	.190	.185	.179	.172	.163	.154
6.00	.176	.175	.173	.170	.166	.161	.154	.146	.137

TABLE IV(b). - NORMALIZED NET FLUX FUNCTION $f(z, \tau, a)$

AT THE MARTIAN SURFACE

Optical depth, τ	Albedo 0.4								
	Zenith angle z , deg								
	45	50	55	60	65	70	75	80	85
0.10	0.586	0.583	0.579	0.575	0.568	0.558	0.540	0.509	0.430
.15	.579	.575	.569	.563	.553	.539	.514	.473	.382
.20	.571	.566	.559	.551	.538	.520	.490	.441	.344
.25	.564	.558	.549	.539	.524	.502	.467	.413	.316
.30	.557	.549	.539	.527	.509	.485	.447	.389	.295
.35	.549	.541	.529	.515	.496	.469	.428	.368	.278
.40	.542	.532	.519	.504	.483	.454	.411	.350	.264
.45	.534	.524	.510	.494	.471	.440	.394	.333	.252
.50	.526	.515	.501	.483	.459	.426	.379	.318	.242
.55	.519	.507	.491	.473	.448	.413	.365	.304	.233
.60	.512	.498	.482	.462	.437	.401	.352	.292	.225
.65	.505	.490	.473	.452	.427	.390	.340	.282	.219
.70	.498	.483	.465	.443	.417	.379	.329	.273	.213
.75	.491	.475	.456	.434	.407	.368	.318	.264	.207
.80	.483	.467	.448	.425	.397	.358	.308	.256	.202
.85	.476	.459	.440	.416	.389	.349	.300	.249	.198
.90	.470	.452	.432	.408	.380	.341	.292	.242	.193
.95	.463	.445	.424	.400	.371	.332	.283	.235	.189
1.00	.456	.438	.417	.392	.362	.323	.276	.228	.184
1.05	.450	.431	.410	.384	.354	.316	.270	.223	.180
1.10	.443	.424	.402	.377	.347	.309	.264	.219	.177
1.15	.437	.417	.396	.370	.339	.302	.258	.214	.174
1.20	.431	.411	.389	.363	.332	.295	.252	.209	.171
1.25	.424	.404	.382	.356	.324	.288	.246	.204	.167
1.30	.417	.398	.376	.349	.317	.281	.240	.200	.164
1.35	.412	.392	.370	.343	.311	.276	.236	.197	.162
1.40	.406	.386	.363	.337	.306	.271	.232	.193	.159
1.45	.400	.380	.357	.331	.300	.265	.227	.190	.157
1.50	.395	.374	.351	.325	.294	.260	.223	.186	.154
1.55	.389	.368	.346	.319	.288	.255	.219	.183	.152
1.60	.384	.363	.340	.313	.283	.250	.215	.180	.149
1.65	.378	.357	.334	.307	.277	.245	.211	.176	.147
1.70	.372	.352	.329	.302	.272	.240	.206	.173	.144
1.75	.367	.347	.324	.297	.267	.236	.203	.171	.142
1.80	.363	.342	.319	.292	.263	.232	.200	.168	.140
1.85	.358	.337	.314	.287	.258	.228	.197	.166	.138
1.90	.353	.332	.309	.283	.254	.224	.193	.163	.136
1.95	.348	.327	.304	.278	.250	.220	.190	.161	.134
2.00	.343	.322	.299	.273	.245	.217	.187	.158	.133
2.10	.333	.312	.289	.264	.237	.209	.181	.153	.129
2.20	.323	.303	.281	.256	.229	.202	.175	.149	.126
2.30	.315	.295	.273	.248	.222	.196	.170	.145	.122
2.40	.307	.287	.265	.241	.216	.191	.166	.142	.119
2.50	.299	.279	.257	.234	.209	.185	.161	.138	.116
2.60	.291	.271	.249	.227	.203	.179	.156	.134	.113
2.70	.283	.263	.242	.220	.197	.174	.151	.130	.110
2.80	.275	.255	.234	.213	.191	.169	.147	.127	.107
2.90	.268	.249	.228	.207	.186	.165	.144	.124	.104
3.00	.261	.243	.223	.202	.182	.161	.141	.121	.102
3.20	.249	.231	.211	.192	.172	.153	.134	.115	.097
3.40	.235	.218	.200	.181	.163	.145	.127	.110	.093
3.60	.223	.207	.189	.171	.154	.137	.121	.104	.089
3.80	.213	.197	.181	.164	.147	.131	.115	.100	.086
4.00	.204	.189	.173	.157	.141	.125	.110	.096	.082
4.50	.182	.168	.154	.140	.126	.112	.099	.087	.074
5.00	.161	.149	.136	.124	.113	.101	.090	.078	.066
5.50	.143	.133	.121	.110	.100	.091	.080	.070	.059
6.00	.128	.119	.109	.099	.090	.081	.072	.063	.054

TABLE V. - NORMALIZED NET FLUX FUNCTION COEFFICIENTS, $f(z, \tau, \alpha)$

k = 0						
i \ j	0	1	2	3	4	5
0	1.002800	-0.228681	0.019613	0.000231	-0.000130	0.000003
1	-.450073	1.335955	-1.131691	.402126	-.063967	.003758
2	5.566705	-16.912405	13.739701	-4.756079	.743740	-.043159
3	-22.471579	64.909973	-52.509470	17.997548	-2.786548	.160340
4	36.334497	-101.800319	79.895539	-26.762885	4.074117	-.231476
5	-20.420490	53.207148	-39.949537	12.977108	-1.931169	.107837

k = 1						
i \ j	0	1	2	3	4	5
0	0.009814	0.226139	-0.117733	0.030579	-0.004090	0.000218
1	-.156701	.396821	-.313648	.099227	-.013508	.000651
2	1.361122	-3.758111	3.007907	-.987457	.141693	-.007320
3	-4.365924	12.539251	-10.394165	3.486452	-.513123	.027401
4	5.991693	-17.498138	14.291370	-4.765323	.703675	-.037960
5	-2.915099	8.275686	-6.593125	2.173999	-.320308	.017335

TABLE VI. - PERCENT OCCURRENCE PROBABILITY OF A LOCAL DUST STORM

Latitude, deg	L_s , deg									
	0 to 45	45 to 80	80 to 125	125 to 160	160 to 200	200 to 245	245 to 270	270 to 290	290 to 325	325 to 360
-90 to -60	2.816	1.583	0.000	0.000	3.079	6.166	6.852	4.111	4.756	1.541
-60 to -30	.706	.399	.197	.928	1.368	1.968	1.754	1.289	1.426	.418
-30 to 0	.262	.703	.323	.227	.359	.594	1.156	.648	.966	.383
0 to 30	.238	.703	.645	.620	.497	.514	.774	.433	.716	.414
30 to 60	.527	.654	.806	1.022	1.044	1.177	1.304	1.756	.967	.903
60 to 90	3.494	2.401	2.372	2.668	4.275	5.483	.000	.000	.000	.000

TABLE VII. - NUMBER OF
DAYS WITH A LOCAL
DUST STORM IN A
MARTIAN YEAR

Latitude bin, deg	Days, L_s , deg
-90 to -60	10.57
-60 to -30	3.65
-30 to 0	1.89
0 to 30	1.97
30 to 60	3.47
60 to 90	8.59

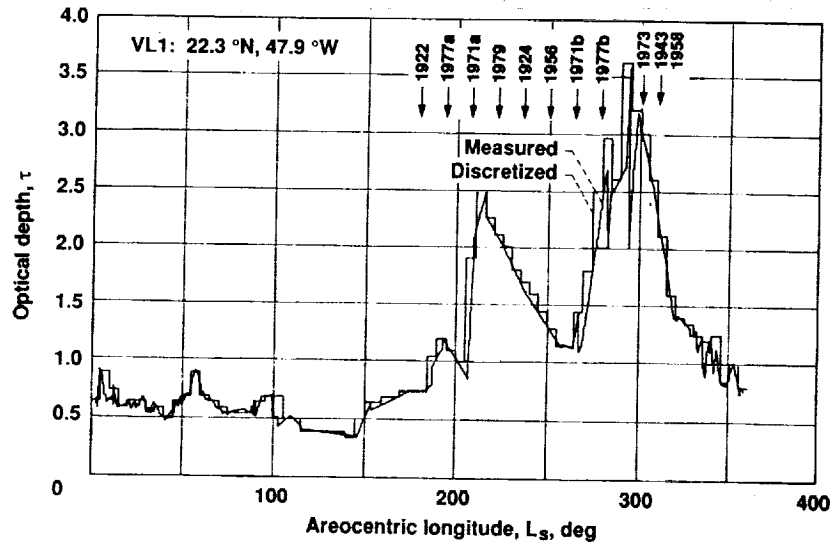


Fig. 1 - Measured and discretized optical depth at Viking Lander VL1 and years of great dust storms.

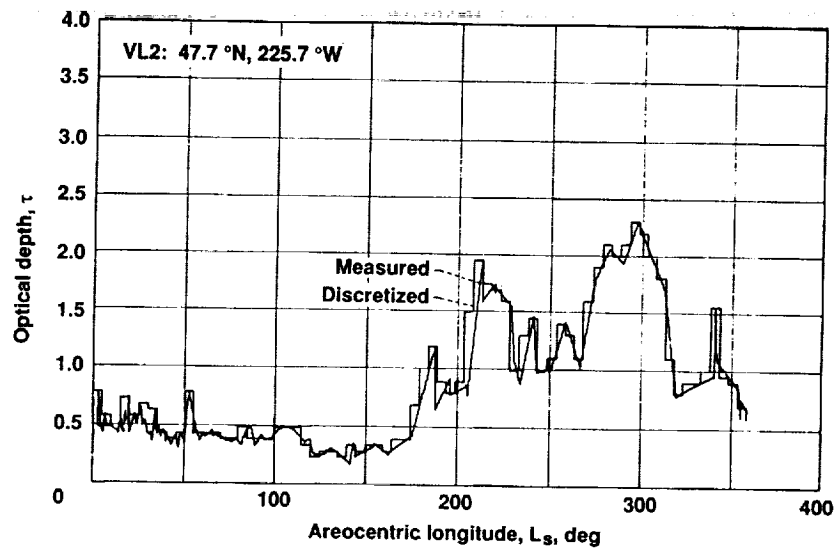


Fig. 2 - Measured and discretized optical depth at Viking Lander VL2

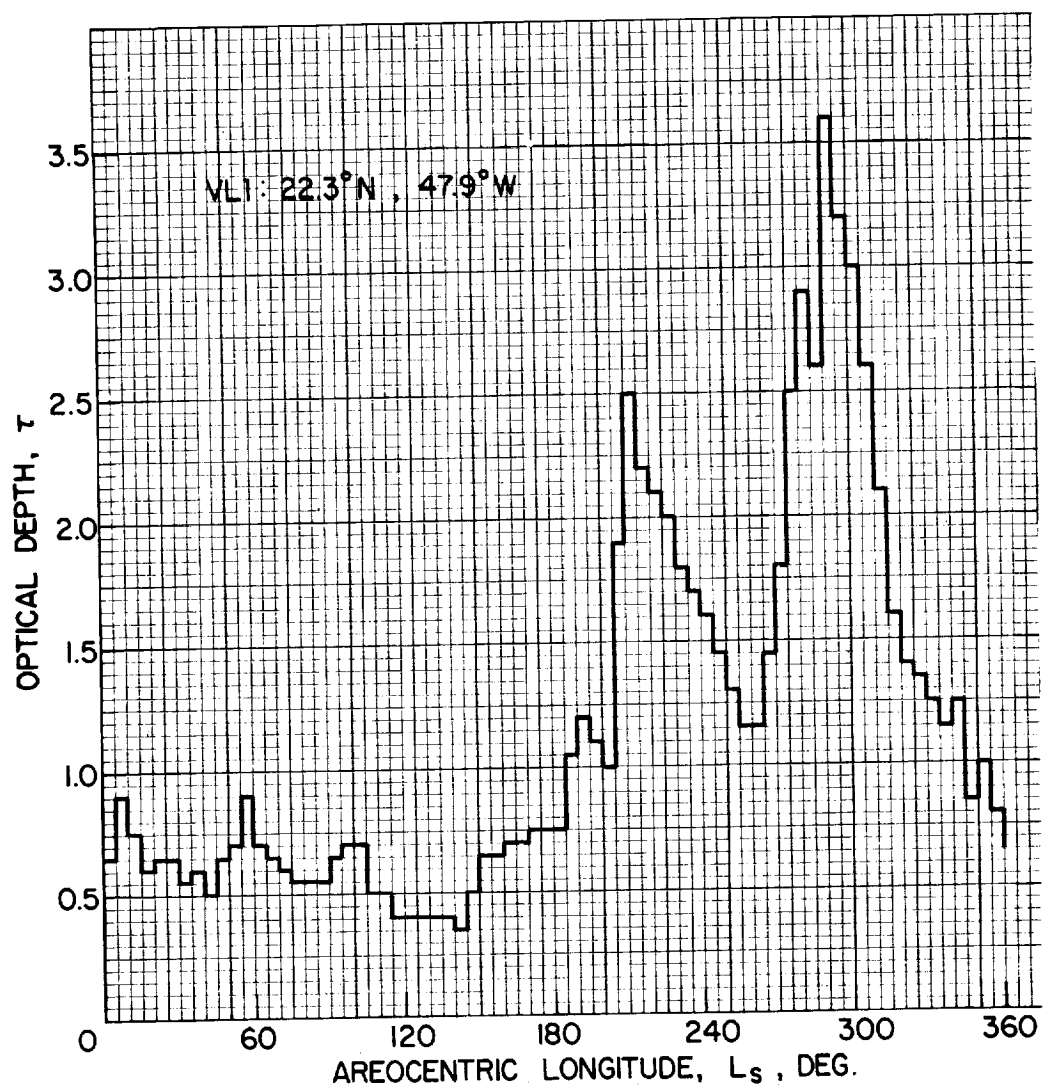


Fig. 3 - Optical depth at Viking Lander VL1 - in detail.

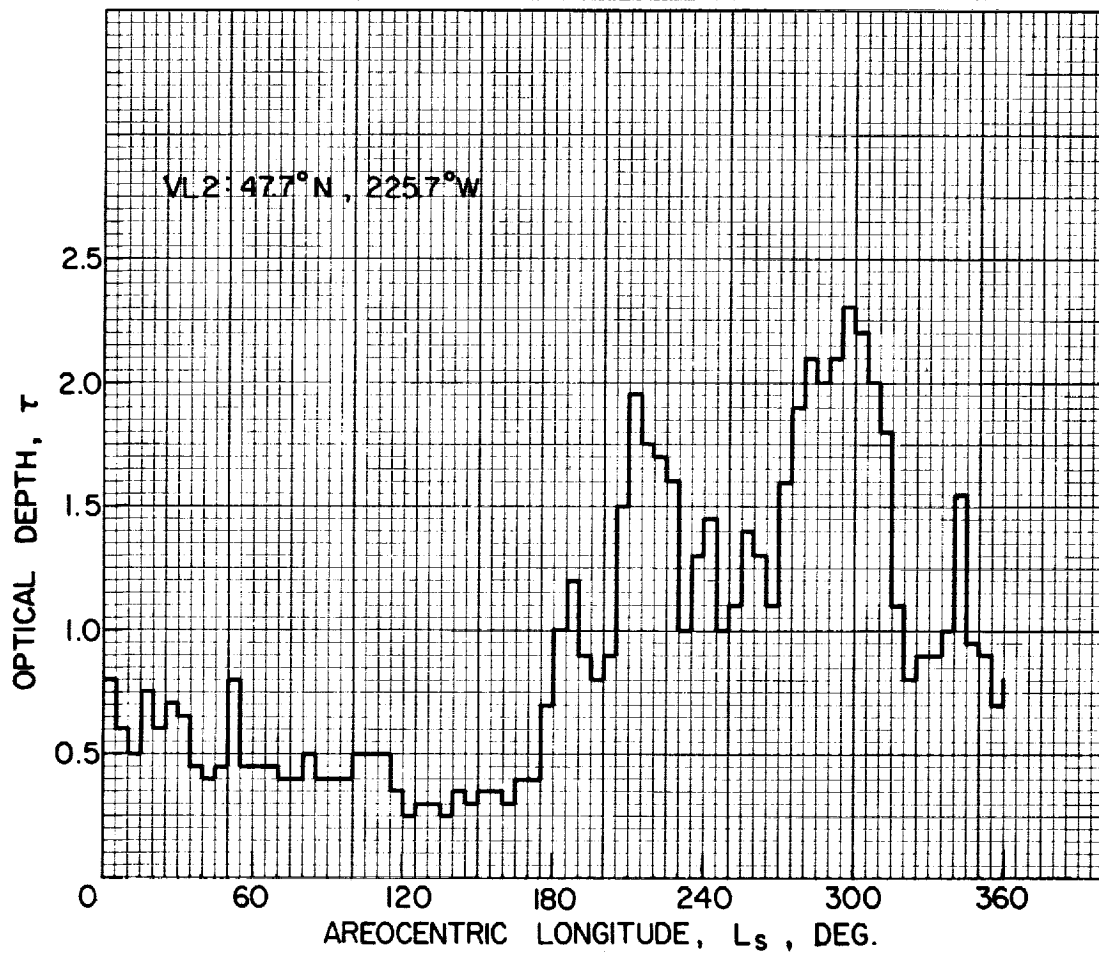


Fig. 4 - Optical depth at Viking Lander VL2 - in detail.

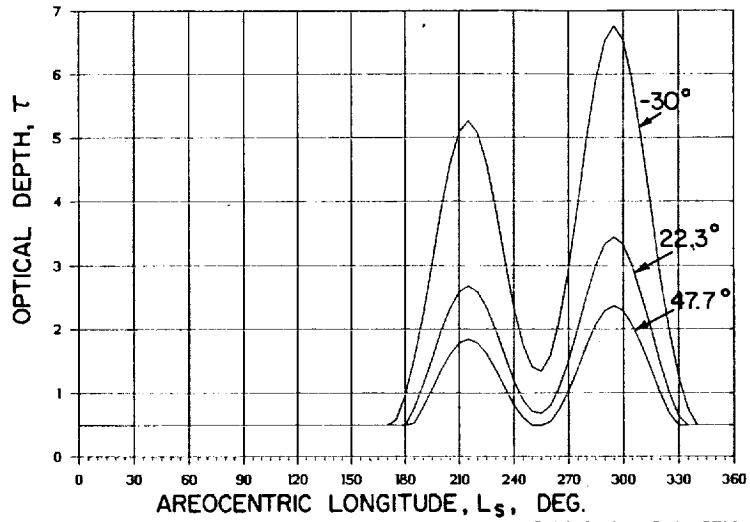


Fig. 5 - Variation of optical depth with areocentric longitude for latitudes of the Viking Landers VL1 (22.3°N) and VL2 (47.7°N), and for the latitude -30° of the two global storm sources.

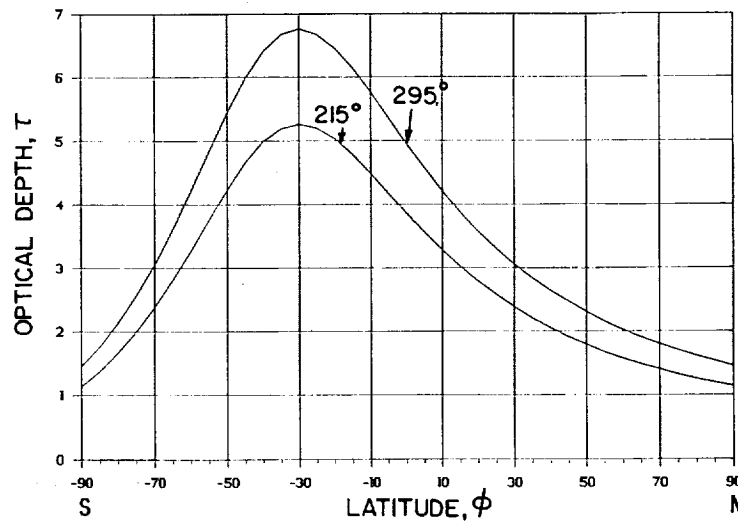


Fig. 6 - Variation of optical depth with latitude at areocentric longitude of the first ($L_s=215^\circ$) and the second ($L_s=295^\circ$) global storms.

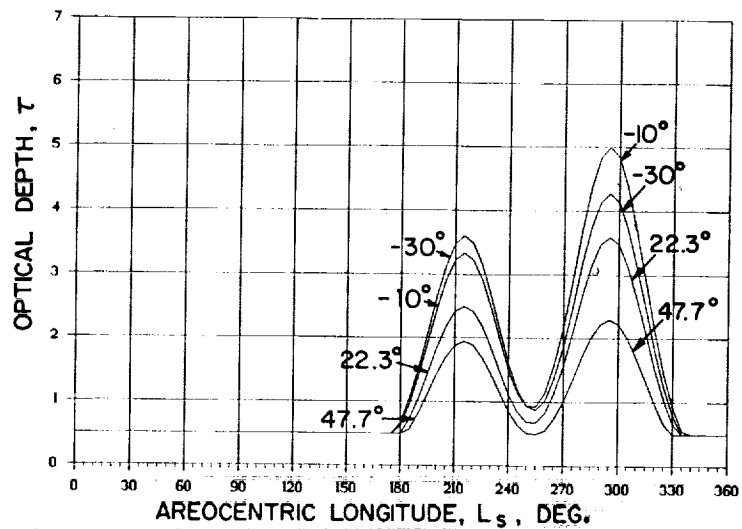


Fig. 7 - Variation of optical depth with areocentric longitude for latitudes of the Viking Landers VL1 (22.3°N) and VL2 (47.7°N), and for the latitude of the first -30° and for the second -10° global storm sources.

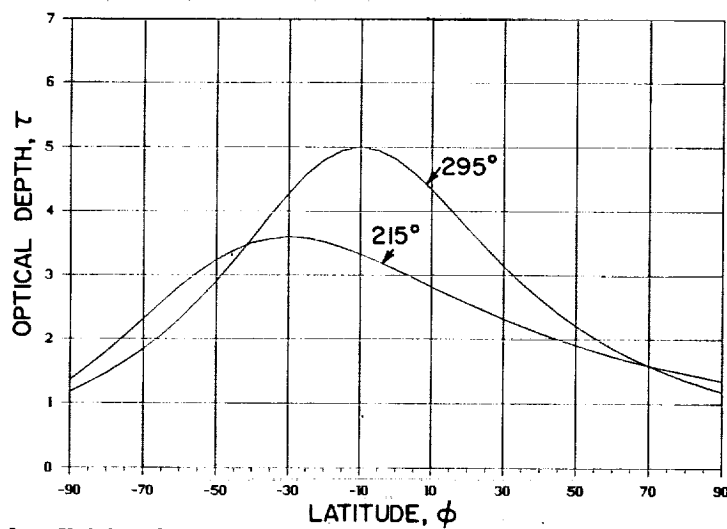


Fig. 8 - Variation of optical depth with latitude at areocentric longitude of the first ($L_s=215^\circ$) and the second ($L_s=295^\circ$) global storms.

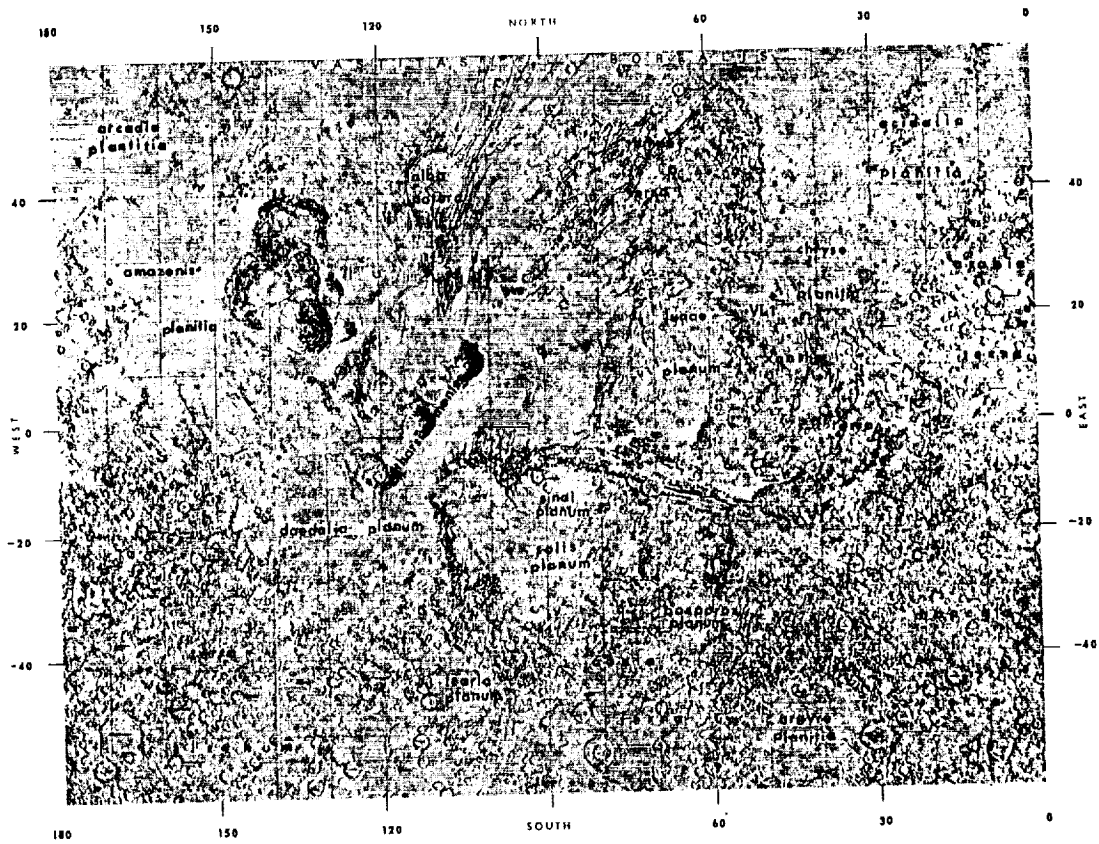


FIGURE 9a. - MARS MAP, 1:15,000,000, IN PART OF THE INTERIOR, U.S. GEOLOGICAL SURVEY.

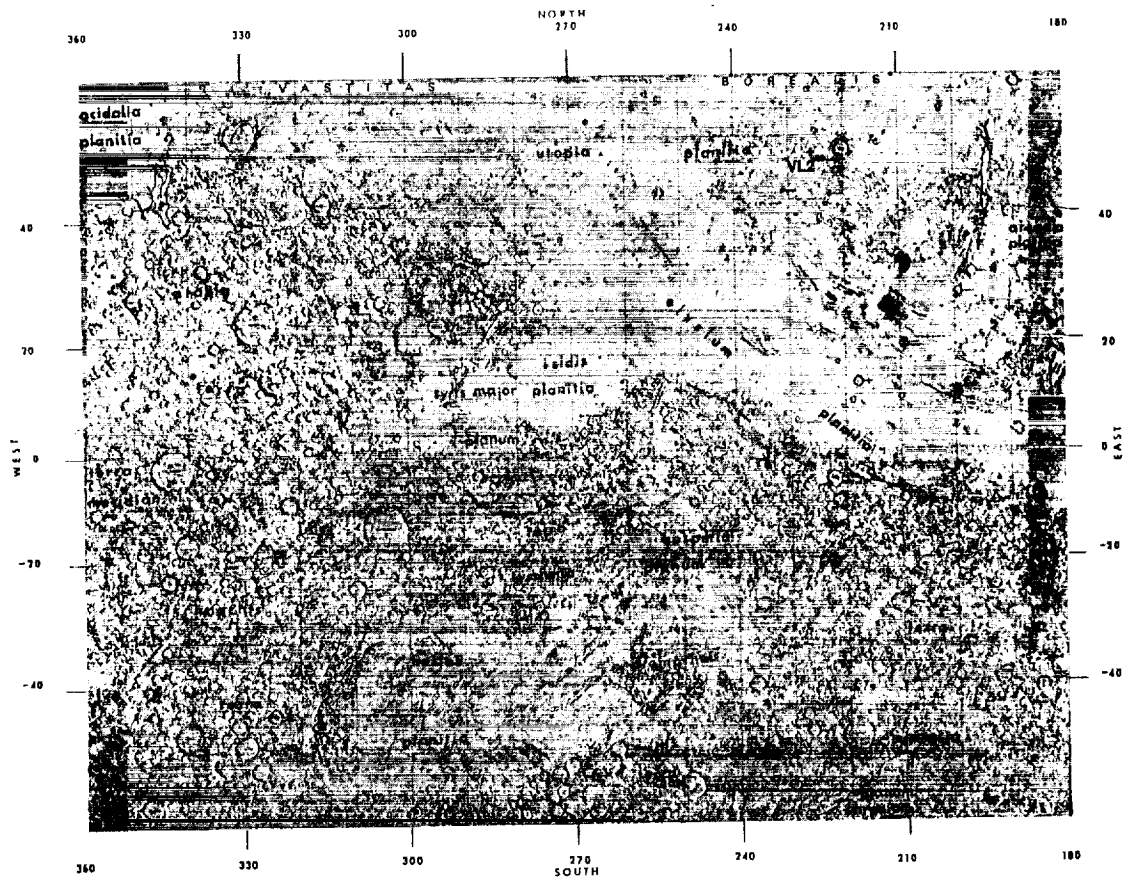


FIGURE 9b. - MARS MAP, 1:15,000,000, IN PART OF THE INTERIOR, U.S. GEOLOGICAL SURVEY.

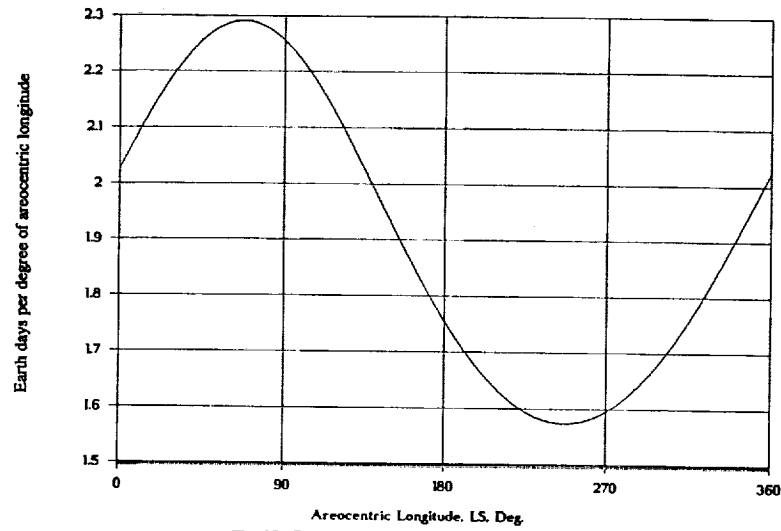


Fig. 10 - Earth days per one degree of areocentric longitude.

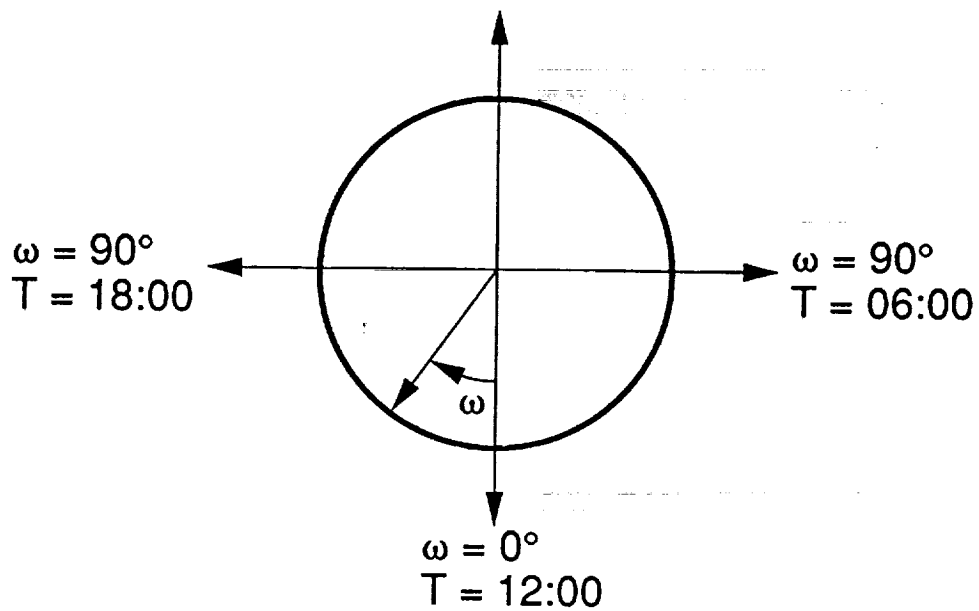
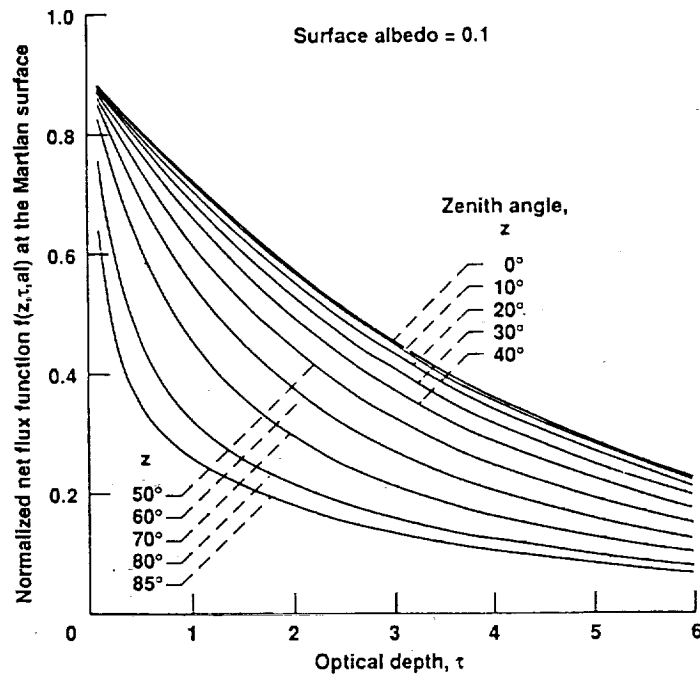
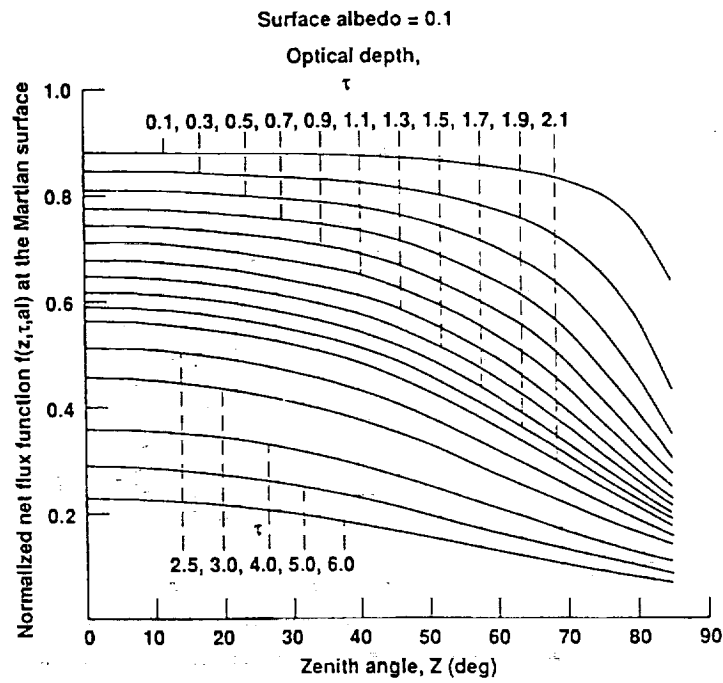


Fig. 11 - Solar time and hour angle relation.

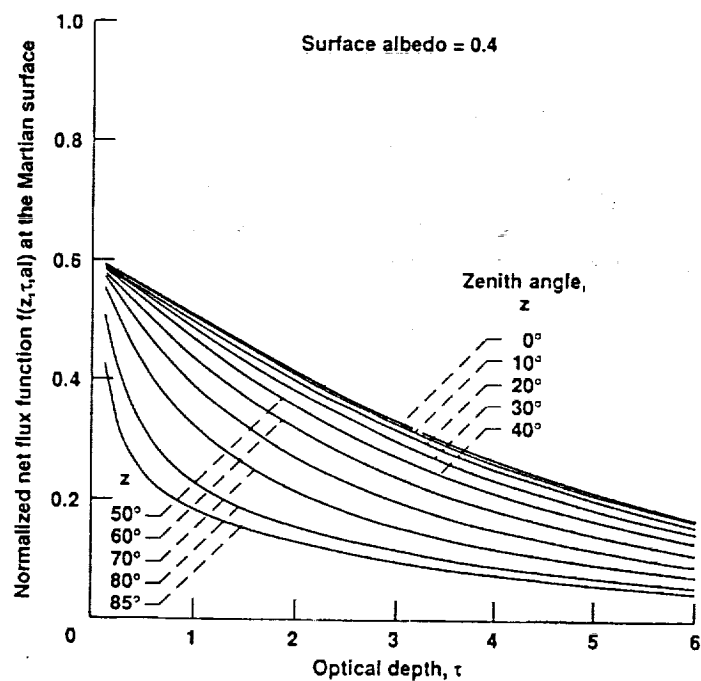


(a) Effect of optical depth with Sun zenith angle as a parameter

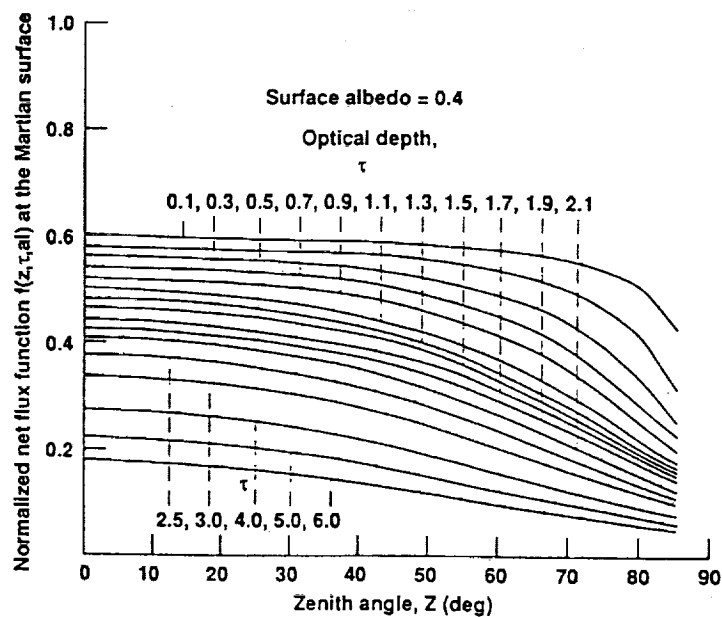


(b) Effect of Sun zenith angle with optical depth as a parameter

Fig. 12 - Variation of the normalized net flux function at the Martian surface with optical depth and Sun zenith angle, for albedo = 0.1

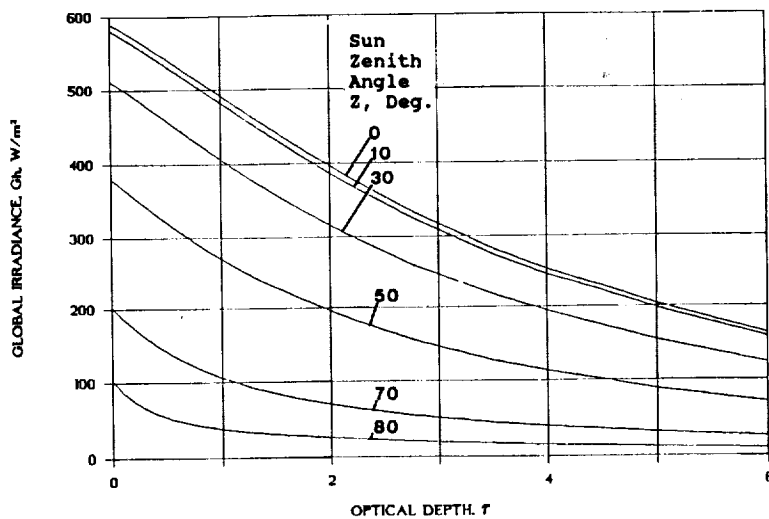


(a) Effect of optical depth with Sun zenith angle as a parameter

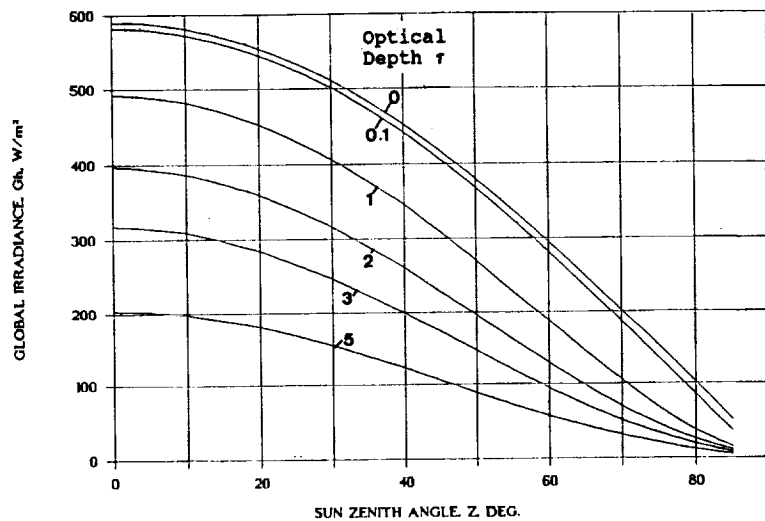


(b) Effect of Sun zenith angle with optical depth as a parameter

Fig. 13 - Variation of the normalized net Flux function at the Martian surface with optical depth and Sun zenith angle, for albedo = 0.4

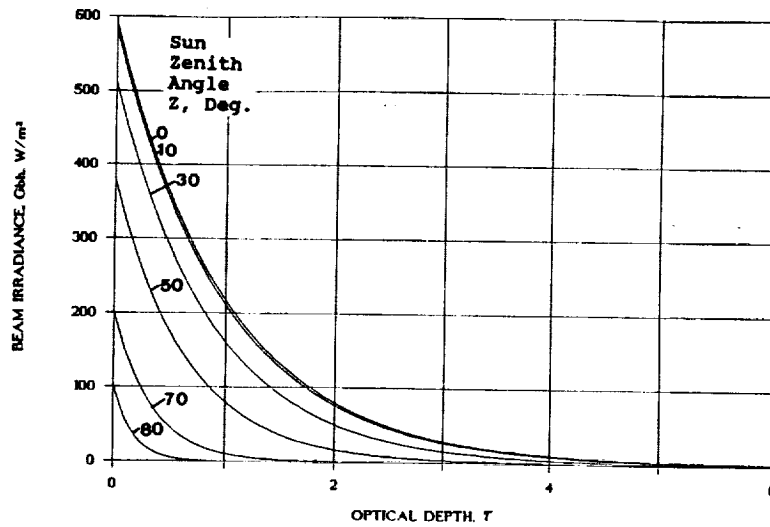


(a) Effect of optical depth with Sun zenith angle as a parameter

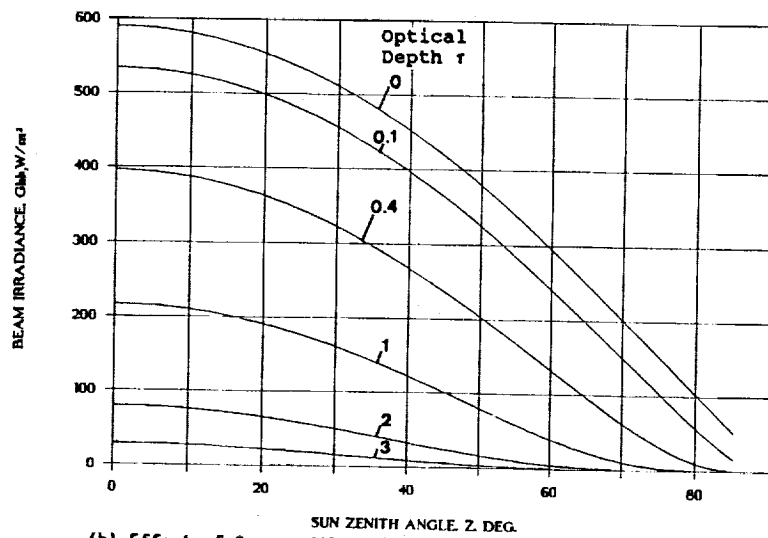


(b) Effect of Sun zenith angle with optical depth as a parameter

Fig. 14 - Variation of the global irradiance with optical depth and Sun zenith angle on a horizontal surface, at mean irradiance of 590 W/m^2

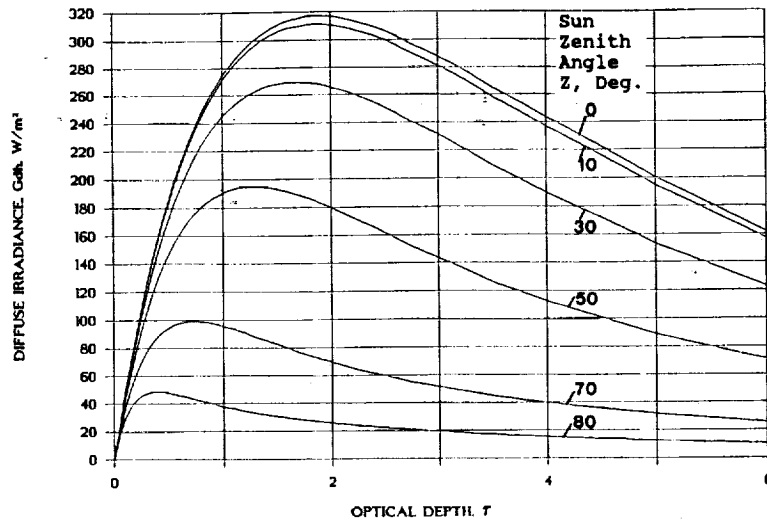


(a) Effect of optical depth with Sun zenith angle as a parameter

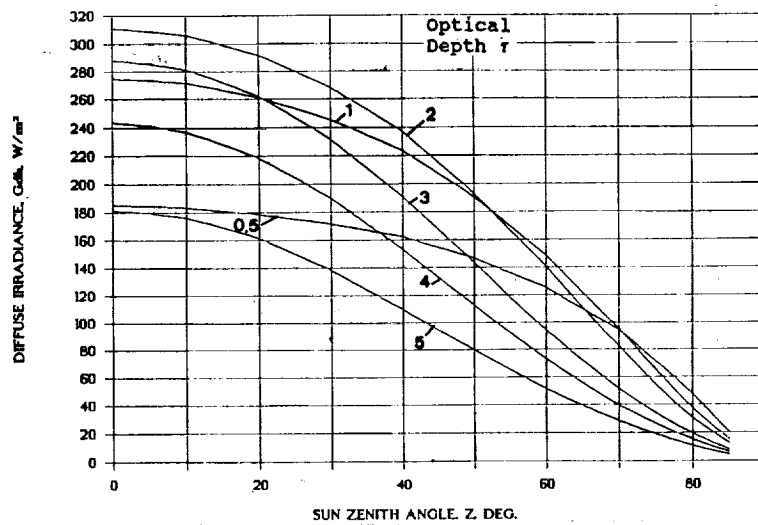


(b) Effect of Sun zenith angle with optical depth as a parameter

Fig. 15 - Variation of beam irradiance with optical depth and Sun zenith angle, on a horizontal surface, at mean irradiance of $590 W/m^2$

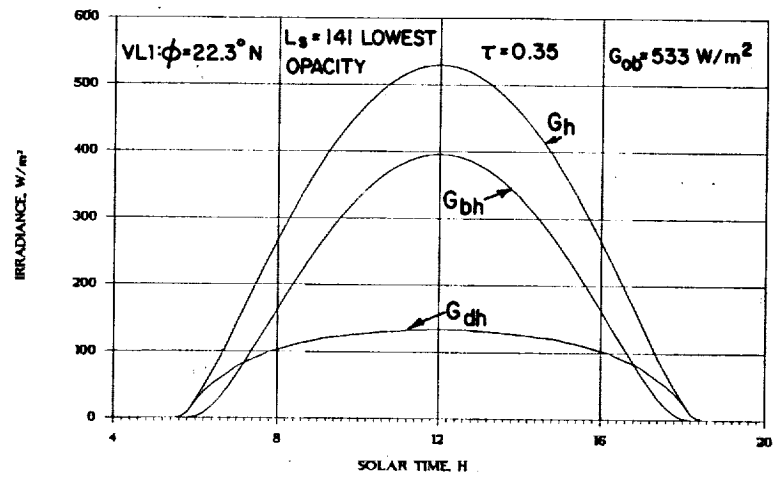


(a) Effect of optical depth with Sun zenith angle as a parameter

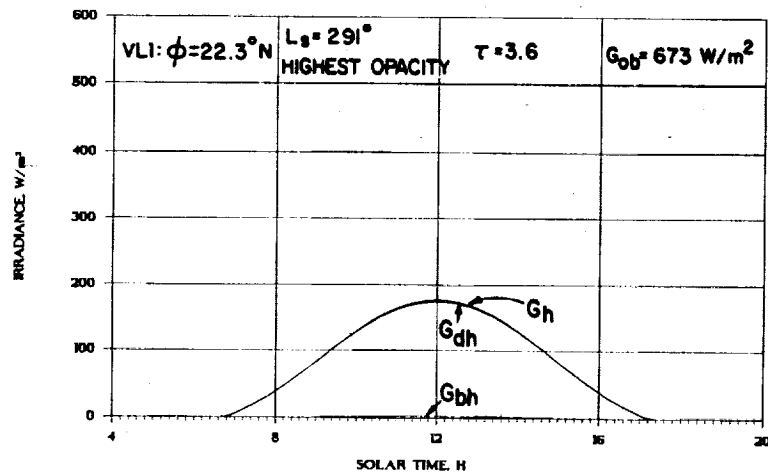


(b) Effect of Sun zenith angle with optical depth as a parameter

Fig. 16 - Variation of diffuse irradiance with optical depth and sun zenith angle, on a horizontal surface, at mean irradiance of $590 W/m^2$



(a) For $L_s = 141^\circ$ and $\tau = 0.35$ (lowest opacity).



(b) For $L_s = 291^\circ$ and $\tau = 3.60$ (highest opacity).

Fig. 17 - Diurnal variation of global G_h , beam G_{bh} , and diffuse G_{dh} irradiance on a horizontal Mars surface at Viking Lander VL1.

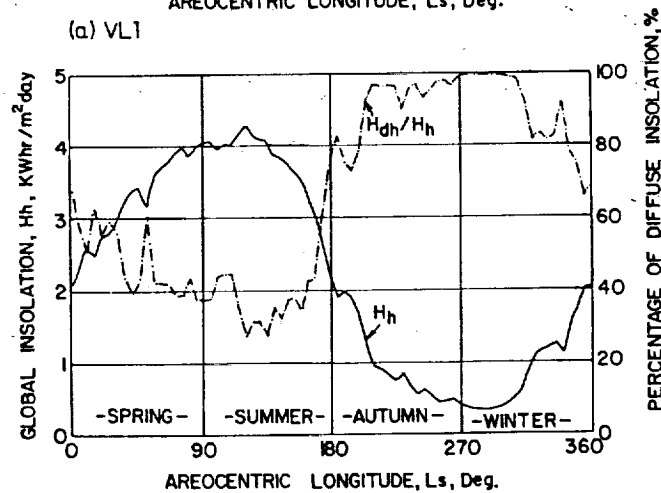
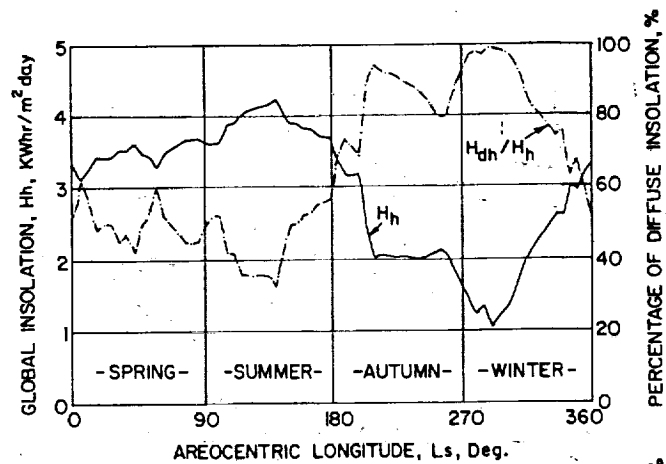


Fig. 18 - Daily global insolation H_h and percentage of diffuse insolation H_{dh}/H_h on a horizontal surface on Mars at VL1 and VL2.

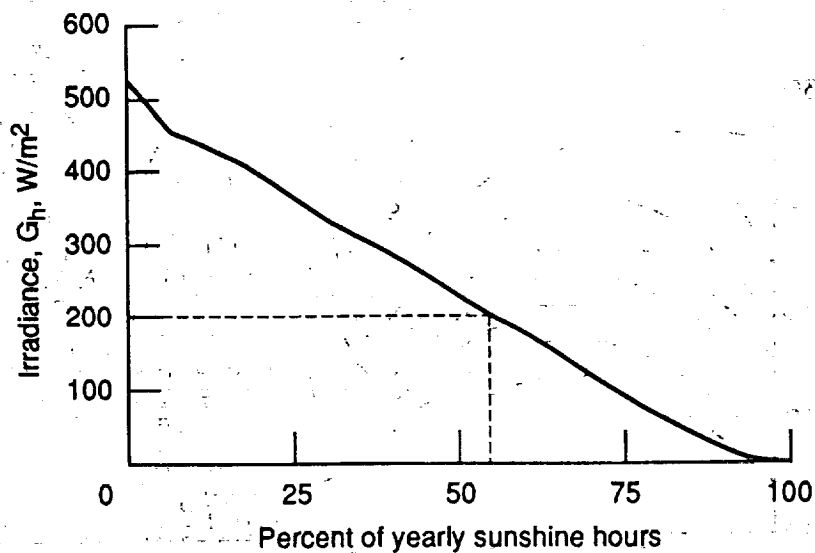


Fig. 19 - Cumulative irradiance on a horizontal surface at VL1 for a Mars year.

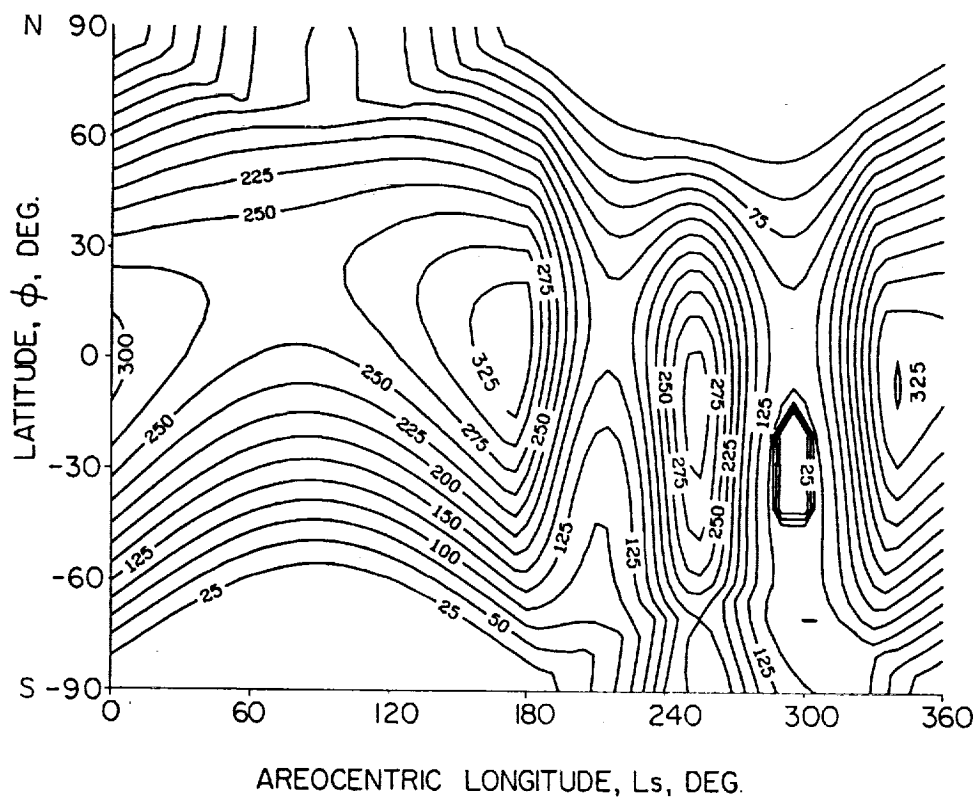


Fig. 20 - Variation of global irradiance G_h (W/m²) with latitude and areocentric longitude on a horizontal surface of Mars based on the optical depth function eq. (1).

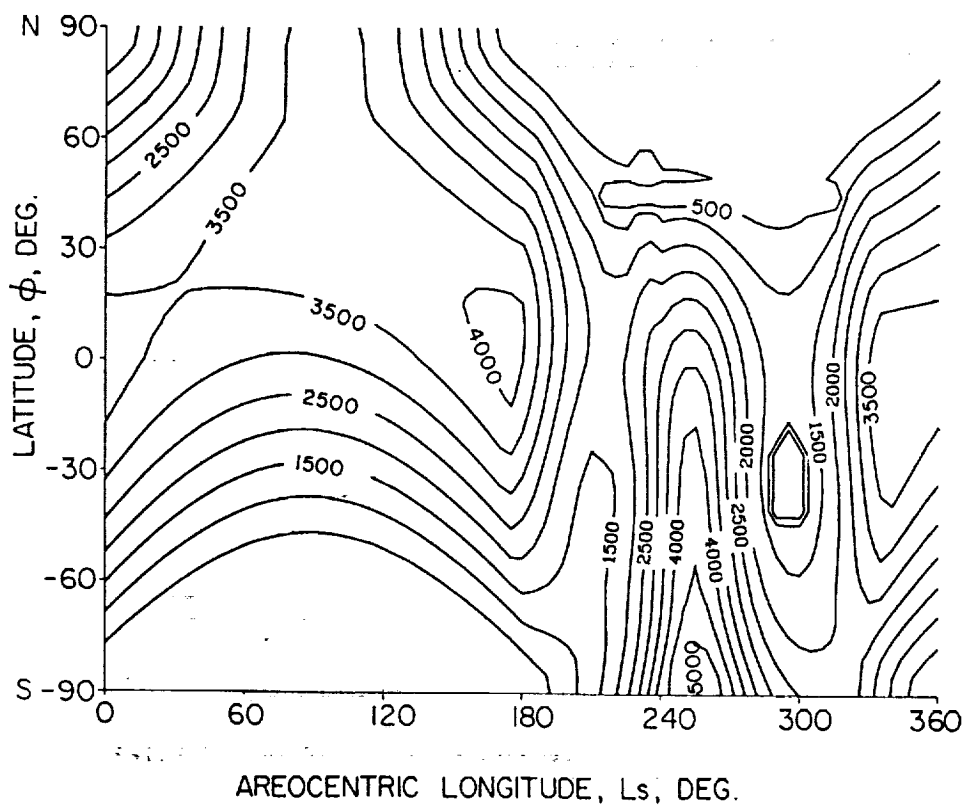


Fig. 21 - Variation of daily global insolation H_0 (Whr/m² day) with latitude and areocentric longitude on a horizontal surface of Mars based on the optical depth function eq. (1).

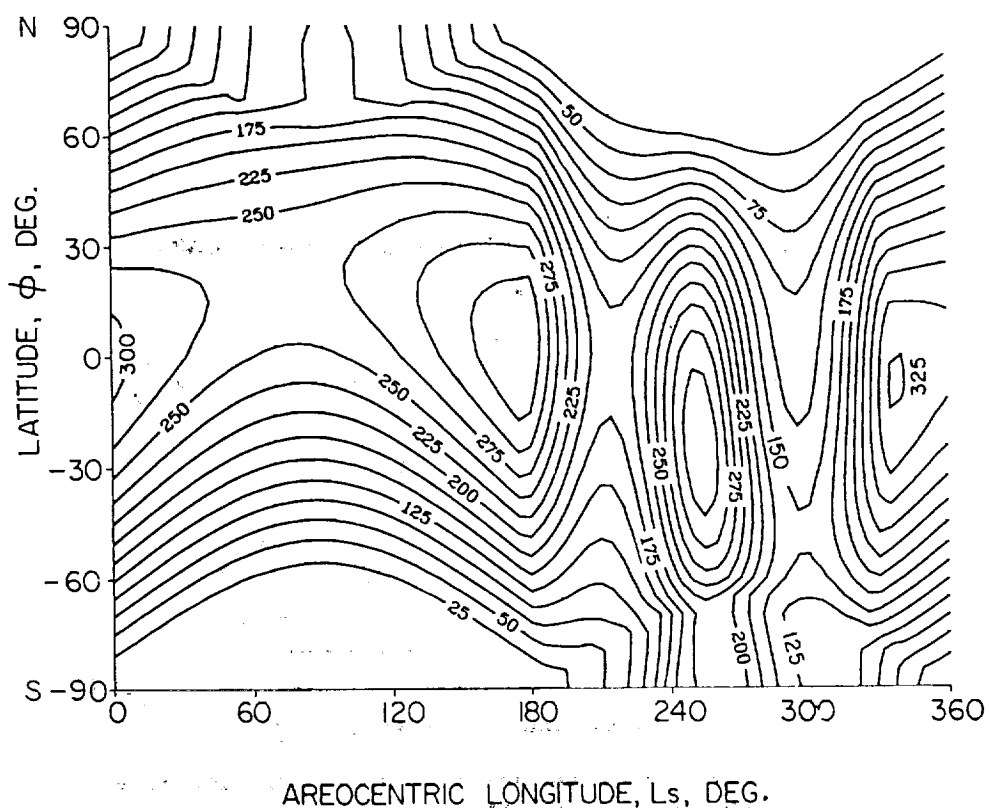


Fig. 22 - Variation of global irradiance G_h (W/m²) with latitude and areocentric longitude on a horizontal surface of Mars based on the optical depth function eq. (2).

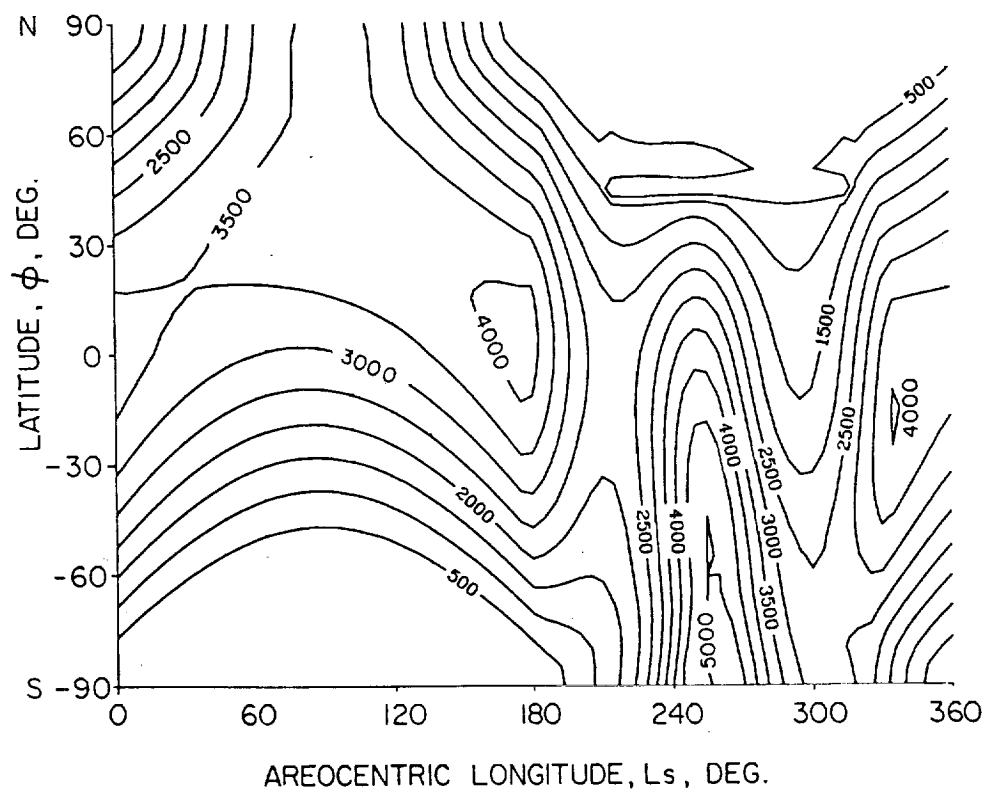


Fig. 23 - Variation of daily global insolation H_h (Whr/m² day) with latitude and areocentric longitude on a horizontal surface of Mars based on the optical depth function eq. (2).

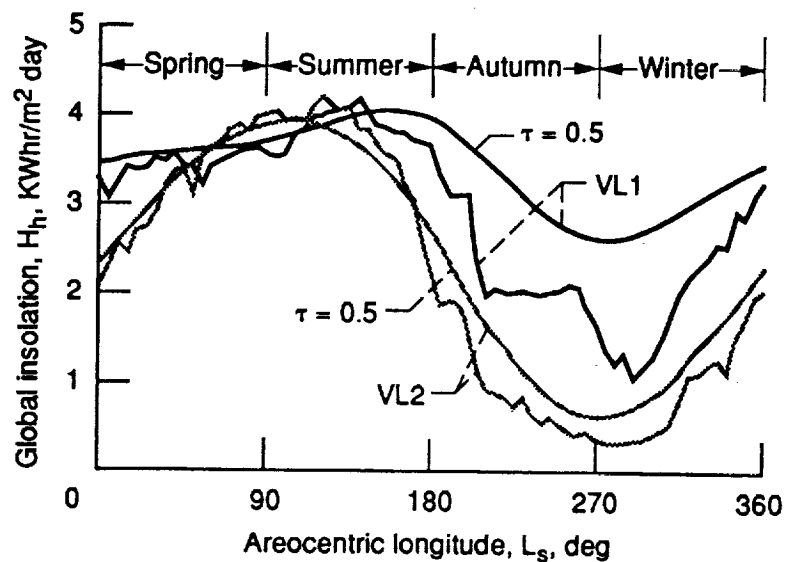


Fig. 24 - Daily global insolation at VL1 and VL2 for the observed opacities at VL1 and VL2 and for $\tau = 0.5$.

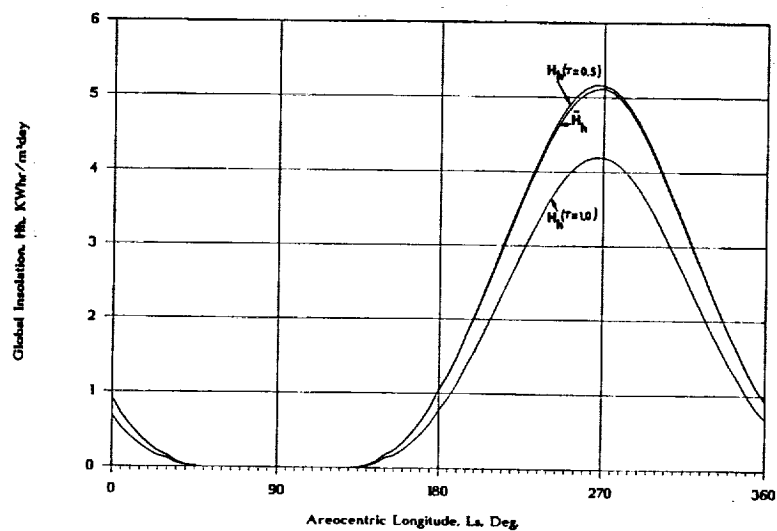


Fig. 25 - The effect of local dust storms on the daily global insolation on a horizontal surface at latitude of 70° S.

REPORT DOCUMENTATION PAGE			Form Approved OMB No. 0704-0188	
Public reporting burden for this collection of information is estimated to average 1 hour per response, including the time for reviewing instructions, searching existing data sources, gathering and maintaining the data needed, and completing and reviewing the collection of information. Send comments regarding this burden estimate or any other aspect of this collection of information, including suggestions for reducing this burden, to Washington Headquarters Services, Directorate for Information Operations and Reports, 1215 Jefferson Davis Highway, Suite 1204, Arlington, VA 22202-4302, and to the Office of Management and Budget, Paperwork Reduction Project (0704-0188), Washington, DC 20503.				
1. AGENCY USE ONLY (Leave blank)	2. REPORT DATE September 1991	3. REPORT TYPE AND DATES COVERED Technical Memorandum		
4. TITLE AND SUBTITLE Solar Radiation on Mars—Update 1991		5. FUNDING NUMBERS WU-506-41-11		
6. AUTHOR(S) Joseph Appelbaum and Geoffrey A. Landis				
7. PERFORMING ORGANIZATION NAME(S) AND ADDRESS(ES) National Aeronautics and Space Administration Lewis Research Center Cleveland, Ohio 44135-3191		8. PERFORMING ORGANIZATION REPORT NUMBER E-6465		
9. SPONSORING/MONITORING AGENCY NAMES(S) AND ADDRESS(ES) National Aeronautics and Space Administration Washington, D.C. 20546-0001		10. SPONSORING/MONITORING AGENCY REPORT NUMBER NASA TM-105216		
11. SUPPLEMENTARY NOTES Portions of this material were presented at the European Space Power Conference sponsored by the European Space Agency, Florence, Italy, September 2-6, 1991. Joseph Appelbaum, National Research Council—NASA Research Associate, on leave from Tel Aviv University, Tel Aviv 69978 Israel (work funded by NASA Grant NAGW-2022). Geoffrey A. Landis, Sverdrup Technology, Inc., Lewis Research Center Group, 2001 Aerospace Parkway, Brook Park, Ohio 44142 (work funded by NASA Contract NAS3-25266). Responsible person, Geoffrey A. Landis, (216) 433-2238.				
12a. DISTRIBUTION/AVAILABILITY STATEMENT Unclassified - Unlimited Subject Category 92		12b. DISTRIBUTION CODE		
13. ABSTRACT (Maximum 200 words) Detailed information on solar radiation characteristics on Mars are necessary for effective design of future planned solar energy systems operating on the surface of Mars. In this paper we present a procedure and solar radiation related data from which the daily variation of the global, direct beam and diffuse insolation on Mars are calculated. Given the optical depth of the Mars atmosphere, the global radiation is calculated from the normalized net flux function based on multiple wavelength and multiple scattering of the solar radiation. The direct beam was derived from the optical depth using Beer's law, and the diffuse component was obtained from the difference of the global and the direct beam radiation. The optical depths of the Mars atmosphere were derived from images taken of the Sun with a special diode on the cameras used on the two Viking Landers.				
14. SUBJECT TERMS Mars; Optical thickness; Solar radiation; Dust storms; Albedo			15. NUMBER OF PAGES 48	
			16. PRICE CODE A03	
17. SECURITY CLASSIFICATION OF REPORT Unclassified	18. SECURITY CLASSIFICATION OF THIS PAGE Unclassified	19. SECURITY CLASSIFICATION OF ABSTRACT Unclassified	20. LIMITATION OF ABSTRACT	

